Research Square

Preprints are preliminary reports that have not undergone peer review.
They should not be considered conclusive, used to inform clinical practice,
or referenced by the media as validated information.

Green Synthesis of Silver Nanoparticles-Coated Chitosan Modified Screen Printed Carbon Electrode and Its Application to The Simultaneous Determination of Cd and Cu by Cyclic Voltammetry

Rachmin Munadi

rachminmunadi.dpk@uim-makassar.ac.id

Islamic University of Makassar

Abdul Wahid Wahab

Hasanuddin University

Abdul Karim

Hasanuddin University

Fatimah Fatimah

STIKES Panrita Husada

Research Article

Keywords: AgNPs, Chitosan, Cadmium, Copper, SPCE, Cyclic Voltammetry

Posted Date: April 10th, 2026

DOI: https://doi.org/10.21203/rs.3.rs-8947871/v1

License: This work is licensed under a Creative Commons Attribution 4.0 International License.
Read Full License

Additional Declarations: No competing interests reported.

Green Synthesis of Silver Nanoparticles-Coated Chitosan Modified Screen Printed Carbon Electrode and Its Application to The Simultaneous Determination of Cd and Cu by Cyclic Voltammetry

Rachmin Munadi[1*], Abdul Wahid Wahab[2], Abdul Karim[2], Fatimah Fatimah[3]

Rachmin Munadi
rachmin.munadi@gmail.com

[1] Department of Chemistry, Islamic University of Makassar, Makassar, South Sulawesi, 90245, Indonesia

Abdul Wahid Wahab
wahidwahab@unhas.ac.id

[2] Department of Chemistry, Hasanuddin University, Makassar, South Sulawesi, 90245, Indonesia

Abdul Karim
Karimkimia@yahoo.com

[3] Department of Medical Laboratory Technology, STIKES Panrita Husada, Bulukumba, South Sulawesi, 90245, Indonesia

Fatimah
imadzakwan02@gmail.com

(*Corresponding author's e-mail: rachminmunadi.dpk@uim-makassar.ac.id)

Abstract

Modification of the Screen Printed Carbon Electrode (SPCE) using silver nanoparticles-coated with chitosan (AgNPs-Chi) was performed for the simultaneous determination of Cd and Cu using the cyclic voltametry method. The study aims to synthesize AgNPs in a green manner and modify carbon screen-printed electrodes as sensors for Cd and Cu detection. AgNPs are synthesized using an eco-friendly reducing agent from the water extract of red ginger leaves (*Zingiber officinale* Rosc. var Rubrum). The formation of AgNPs-Chi was visually confirmed by a color change from yellow to brownish-yellow and validated by UV-Visible spectroscopy, which showed a surface plasmon resonance band at 432.5–452.5 nm, which remained stable during the 7-day incubation period. AgNPs-Chi particles have a face-centered cubic shape, an average size of 118 nm, and are well distributed, with a polydispersity index of 0.410. EDX analysis confirmed silver (46.9%) as the dominant element, with several other components, including carbon, oxygen, and nitrogen. The FTIR spectrum confirms the successful integration of chitosan onto the surface of AgNPs. AgNPs-Chi has the potential to be developed as an SPCE modifier for the simultaneous determination of Cd and Cu, providing simple, fast, accurate, and sensitive results using cyclic voltammetry. The detection limits for Cu and Cd were 9.48 ppm and 6.97 ppm, respectively. The sensitivities are 0.25 μAppm-1mm-2 and 0.34 μAppm-1mm-2, respectively. The accuracy is 150.2% and 101.8%, respectively. These findings show that cyclic voltammetry using SPCE/AgNPs-Chi for Cu determination is more sensitive and accurate than Cd.

Keywords : AgNPs ; Chitosan ; Cadmium ; Copper ; SPCE ; Cyclic Voltammetry

1. Introduction

Today, the alarming presence of heavy metals in the environment stems primarily from industrial activities—unlike organic pollutants, they are not biodegradable. Metals such as cadmium pose significant threats due to their high toxicity, whereas copper is vital for physiological processes but is harmful at excessive levels [1]. Therefore, fast, sensitive analytical methods to monitor these ions are needed [2,3]. Traditional techniques, including electrothermal atomic absorption spectrometry (EAAS), flame atomic

absorption spectrometry (FAAS), inductively coupled plasma mass spectrometry (ICP-MS), and inductively coupled plasma (ICP), offer reliability in heavy metal detection [4], but these methods require lengthy analysis, specialized users, and limit portability. Electrochemical techniques, in contrast, are affordable, easy to use, and yield sensitive results quickly with less and smaller equipment [5].

The electrochemical method using voltammetric techniques is a promising alternative for detecting cadmium (Cd) and copper (Cu) in water samples due to its excellent sensitivity, relatively low cost, and short analysis time [6]. Voltammetry measures electrical current as it changes with applied voltage, enabling metal detection. Electrode modification materials, substances added to electrodes to improve their performance, can enhance sensor sensitivity, selectivity, and reusability, drawing researchers' attention. Silver nanoparticles (AgNPs) are key in developing electrochemical sensors. These nanoparticles have optical (interact with light), catalytic (speed up chemical reactions), magnetic, mechanical, and electronic properties, making them useful as sensor materials [7]. AgNPs improve conductivity (facilitating electron flow) and provide more active sites for electron transfer [8]. Their catalytic properties assist oxidation (loss of electrons) and reduction (gain of electrons) reactions [9], increasing selectivity in sensors [7]. Silver nanoparticles are highly sensitive to heavy metals, particularly mercury [10,11].

This study used silver nanoparticles synthesized using red ginger leaf extract (*Zingiber officinale* Rosc. var Rubrum) as a reducing and stabilizing agent. *Zingiber officinale* Rosc. var Rubrum was chosen in this study because it is rich in flavonoid compounds, tannins, terpenoids, and saponins and has strong antioxidant activity (Munadi et al, 2023). Plant extracts contain hydroxyl groups of secondary metabolite compounds such as anthocyanins, flavonoids, polyphenols, carboxylic acids, terpenoids, alkaloids, phenolic acids, proteins, and effective sugars as reducing and covering agents [12,13,14]. Among the plant extracts that have been reported as reducing and covering agents include Centella Asiatica [15,16], Chromolaena odorata [17], Camellia sinensis [18,19], Clitoria ternatea [13], P. longifolia [20], Lavandula stoechas [21], Equisetum diffusum [22], Salvia tiliifolia [23], Rosmarinus officinalis [24], Olea europaea [25], and Coffea canephora [26]. One-step in situ functionalization of AgNPs with phytochemicals promotes their interaction and sensing ability [22]. The hydroxyl and carboxylate groups of secondary metabolites limit particle aggregation at the initial stage [24,25]. The presence of metabolite compounds ensures the electrostatic stability of AgNPs through steric effects [24].

Modifications of AgNPs have been reported to improve the performance of carbon-printed electrodes [28], screen-printed carbon electrodes [29], and graphene electrodes [6] for detecting cadmium contamination at low concentrations. AgNPs-based sensor modifications are suitable for a wide range of analyses [8]. Electrochemical studies revealed that functionalizing AgNPs with 4-mercaptobenzoic acid improved the detection sensitivity of Cu 2+ voltammetry, with a detection limit of 0.08 nM [30]. Cyclic voltammetry modification of rGO-AgNPs enables the sensing of Cd and Cu over a wide concentration range, with low detection limits, high selectivity, and fast response times [31]. Modification of graphite electrodes with AgNPs-Graphene nanoplates increased the sensitivity of Cd and Cu detection by square wave anodic stripping voltammetry (SWASV) with detection limits of 5.0 and 4.1 ng/L, respectively. Some results from this study suggest that silver nanoparticles can be used as supporting nanomaterials in Cd and Cu metal sensors [6].

Incorporating AgNPs (silver nanoparticles) into sensing platforms enhances sensitivity and catalytic performance by increasing active surface area, providing more functional sites for adsorption, and accelerating electron transfer, thereby improving the electrochemical oxidation of target molecules [24]. Modifying cadmium and copper sensors with AgNPs is advantageous, as AgNPs can be synthesized from cost-effective silver nitrate precursors, unlike those required for gold and platinum nanoparticles [9,12]. However, large-scale synthesis may cause AgNPs to agglomerate, reducing homogeneity and stability [7], which affects surface area and catalytic activity. Capping agents—chemicals derived from amphiphilic molecules with polar (water-attracting) and nonpolar (water-repelling) groups—are therefore required [32, 33, 34#_bookmark54]. The polar group bonds to AgNPs, while the nonpolar group interacts with the electrolyte, improving nanoparticle compatibility and preventing agglomeration [7].

The method to overcome agglomeration through capping agents is to use a reducer mediated by plant extracts. Various plant extracts have been reported for this purpose. Green synthesis and stabilization methods using extracts of natural ingredients produce AgNPs with electrochemical activity [25]. AgNPs

produced via green synthesis using natural ingredient extracts exhibit high selectivity for Cd ions and excellent sensitivity, with fast response and detection limits at the part-per-million level [22]. Capping agents can affect detection sensitivity and are key to metal ion detection [35].

AgNPs are functionalized with chitosan capping agents to improve sensitivity for electrochemical sensing applications. Chitosan is a compatible and biodegradable biomaterial [36, 37]. Chitosan is highly stable, selective for heavy metals, and is a good film-forming biopolymer [37]. At low pH, chitosan can facilitate the protonation of amino groups [36], making it possible to interact with silver nanoparticles and various ligands to develop sensor materials [36, 37, 38]. Chitosan matrices can improve selectivity [39, 40, 41], sensitivity, reproducibility, stability, electron transmission rate [37,38,39,40,41,42], and reuse as electrochemical sensors [37].

Modification of silver nanoparticles with ligands, such as polymers such as chitosan, can serve as a stabilizer, affect particle aggregation in an analyte solution (sensor aggregation) [43, 44], and prevent further oxidation of silver to silver oxide [45]. In addition to stabilizing, chitosan-functionalized AgNPs can also be used as sensors for Hg2+ metal ions [46]. Research conducted by [47] using a Screen Printed Carbon Electrode (SPCE) modified with silver/chitosan/carbon nanotube nanoparticles to detect Hg(II) by cyclic voltammetry (CV) yields a linear range of 1.0 nM - 12.6 nM and a detection limit of 0.4 nM. [48] also used carbon glassy electrodes modified with silver/chitosan nanoparticles to detect As(III) by differential pulse anodic stripping voltammetry (DPASV), achieving a detection limit of 11.39 pM. In this study, AgNPs-Chi was used to modify SPCE for the determination of Cd and Cu by CV, a previously unreported method. The CV method is by far the most widely used technique, providing important physical and chemical features, such as redox reactions on the electrode surface, reaction reversibility, insight into reaction mechanisms, kinetics, and adsorption process [47, 49, 50]. Inspired by the good properties of green synthetic silver nanoparticles, the great features of screen printing technology, and the advantages of electrochemical sensing methods in heavy metal analysis, we report, for the first time, the determination of Cu and Cd using chitosan-coated silver nanoparticle-based screen-printing electrodes by Cyclic Voltammetry.

2. Materials and Methods

2.1 Materials

The plant material used in this study is fresh red ginger leaves (*Zingiber officinale* Rosc. var. rubrum) collected from the Makassar Traditional Health Center, Indonesia**.** Other ingredients are AgNO3 (99.8% purity), purchased from Merck; 2% acetic acid, chitosan (Sigma-Aldrich, deacetylation degree ≥ 70%); CH3COONa.3H2O (Merck); Cd(NO3)2.4H2O (Merck); Cu (NO3)2.3H2O (Merck); Whatmann filter paper No. 42; and aluminum foil, double distilled water (Water One). The instruments used in this investigation were analytical scales (Acculab), pH meters (Hanna Instruments HI9813-6), laboratory-standard glassware (Pyrex), heat plates, magnetic stirrers, and freeze-dryers (Buchi 190). The Metrohm Screen Printing Carbon Electrode (DRP-C110-U75) is used in conjunction with the DropSens μStat 400 Potentiostat (DropSens, Spain), which is equipped with the DropView 8400 software for data collection and analysis.

2.2 *Red Ginger Leaf Water Extract Preparation*

The part of the plant used for the synthesis process is the red ginger leaf (**Fig. 1**). Red ginger leaves are harvested in quantities of up to 200 g, thoroughly washed with double-distilled water, and then dried. Once dry, finely chop, weighed to the nearest 5 g, and then brought to a boil in a 250 mL beaker with 100 mL of aquabides, weight ratio of ginger leaves: water (1: 20). After that, the mixture is left to boil for fifteen minutes to maximize the extraction process which can increase the release of bioactive compounds from within the red ginger leaves. Fifteen minutes is considered sufficient to extract phytochemicals from the leaves. Extraction time is too long, which can damage polyphenols and flavonoids in the leaves; if it is too short, the extraction process is suboptimal. This synthesis procedure is in accordance with that carried out by [50], who synthesized silver nanoparticles from bay leaf extract. Whatman paper No. 42 is used to filter the leaf extract solution after it reaches room temperature. The leaf extract solution can be stored in the refrigerator when not in use or immediately used for the synthesis process.



Fig. 1. Red ginger leaf

2.3 Synthesis of Silver Nanoparticles-Coated Chitosan (AgNPs-Chi)

Mix up to 1 mL of red ginger leaf decoction into 90 mL of a 1 mM AgNO3 (Merck) solution (ratio of extract : AgNO3 (1 : 90), stir for 2 hours at room temperature, and observe the solution turn brownish-yellow. The discoloration indicates that silver nanoparticles have formed. A total of 20 mL of the synthesized silver nanoparticles was added to a 0.6 mL 1% chitosan solution in a beaker, and the mixture was stirred for 2 hours with a magnetic stirrer. AgNPs-Chi solutions are characterized using an Ultraviolet -Visible (UV-Vis) Spectrophotometer and PSA. For characterization by FTIR, XRD, and SEM-EDX, the solution is first dried in a freeze dryer at -53°C and 0.8 Mbar.

2.4 Characterization of AgNPs-Chi

The success of synthesized silver nanoparticles (AgNPs-Chi) was determined by characterization using the Visible UV Spectrophotometer (Shimadzu UV-2600), Particle Size Analyzer (PSA) Horiba SZ-100, Fourier Transform Infrared (FTIR) Shimadzu 820 IPC, X-ray Diffraction (XRD) Shimadzu 7000, Scanning Electron Microscopy (SEM) Tescan Vega, and Energy-Dispersive X-ray from the Oxford Instrument (EDX). AgNPs-Chi solutions were characterized using UV-Visible and PSA spectrophotometers, while for characterization by FTIR, XRD, and SEM-EDX, AgNPs-Chi solutions were first dried in a freeze dryer at -53 °C and 0.8 mbar [47]. Characterization using UV-Vis spectrophotometers over 400-700 nm to determine if there is an uptake in the wavelength region characteristic of silver nanoparticles. In addition, UV-Vis spectrophotometry was used to assess the nanoparticles' stability over 7 days. Furthermore, characterization was performed using PSA at 25° and 90° to determine the particle size and distribution of the resulting AgNPs-Chi. Furthermore, AgNPs-Chi was analyzed by FTIR over 4000-500 cm-1 to identify functional groups that play an important role in nanoparticle formation. Further characterization used XRD with Cu Kα radiation and a range of 2θ (35° to 80°), to investigate the crystallinity of AgNPs-Chi. The crystal size of AgNPs-Chi was determined using the Debye-Scherrer equation [50]. The equation can be seen in **Eq. (1)** as follows:

$$D = \frac{k\,l}{\beta\cos\theta} \qquad (1)$$

Where D represents the average size of the crystallite particle , λ represents the X-ray wavelength of 0.154 nm, θ is the Bragg angle, β is the maximum half-width (FWHM), and k = 0.9 represents the form

factor. Furthermore, to determine the surface morphology and elemental composition of AgNPs-Chi, characterization was carried out using SEM-EDX at an Acceleration Voltage of 10 kV and a Magnification of 5000x. The process of synthesis and characterization of AgNPs-Chi is shown schematically in **Fig 2.**

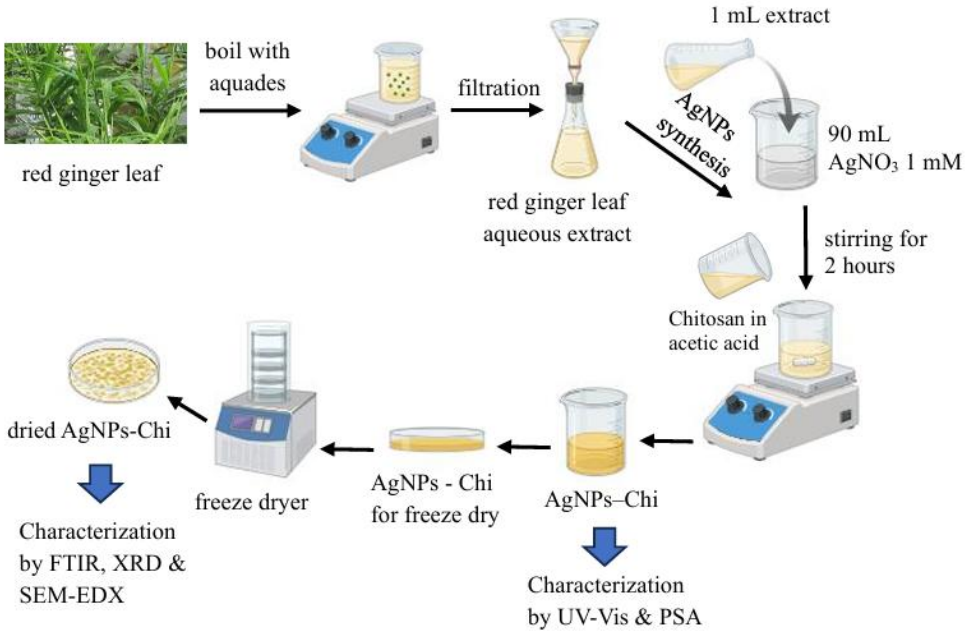


Fig 2. Schematic illustration of the synthesis and characterization of AgNPs-Chi

2.5 Fabrication of Sensor

The SPCE/AgNPs-Chi working electrode is prepared by the drop-casting method: 3 drops of AgNPs-Chi solution are dropped onto the SPCE surface, then dried in the oven for 30 minutes at 50 0C. Furthermore, the electrodes are ready for analysis. Before use for analysis, SPCE/AgNPs-Chi is rinsed with aquaabides. SPCE without AgNPs-Chi is used as a bare electrode (unmodified electrode). The modified electrodes have been rinsed with aquabidest and stored in a dry, sealed container (a dark bottle) to maintain their stability. With proper storage, the electrode will remain stable, preventing oxidation, aggregation, and degradation of the AgNPs-Chi capping layer, thereby maintaining the electrode's catalytic performance [51].

2.6 Electrochemical Measurements for Cd and Cu

Electrochemical measurements for the Cd metal sensor were performed using cyclic voltammetry (CV) with the DropSens µStat 400 Potentiostat (DropSens, Spain) and the DropView 8400 software for data collection. The electrode used is SPCE/AgNPs-Chi (DRP-C110-U75) from Metrohm, which consists of a working electrode and an auxiliary electrode, both carbon, and a reference electrode (Ag/AgCl). The electrochemical treatment of SPCE/AgNPs-Chi was carried out in an acetate buffer solution of 0.1 M, pH 4.5, and a Cd metal solution in a potential range of +0.15 V to -1.1 V, while Cu metal was in a potential range of +1 V to -1 V, with a scan rate of 50 mV/s. CV measurements in Cd metal at a scan rate variation of 40-160 mV/s and a variation in Cd metal concentration at 10-150 ppm. Meanwhile, CV measurements were performed on Cu metal at scan rates of 60-160 mV/s and Cu metal concentrations of 10-125 ppm. The calibration curve is obtained by relating the metal concentration to the peak current. Sensitivity and detection limits are determined from the linear range of each electrode's calibration curve. Measurements were also made on samples of artificial waste.

2.7 Solution Preparation

A 1% chitosan solution is prepared by weighing 0.5 g of chitosan powder, placing it in a beaker, and dissolving it in 30 mL of 2% acetic acid with a magnetic stirrer. Once dissolved, the chitosan solution is put into a 50 mL measuring flask. The volume of the solution is sufficient for a 2% acetic acid solution to the limit line. A 0.1 M pH 4.5 acetate buffer solution is prepared by mixing the corresponding volumes of acu-molar (0.1 M) CH3COONa and CH3COOH solutions in deionized water, and adjusting the pH to 4.5 using 0.1 M HCl and NaOH solutions. A 1000 ppm Cd parent solution is made by carefully weighing 2.74 g of Cd(NO3) 2 · 4H2O, dissolving it in aquabida, and diluting to 1 L. Next, dilutions were performed to obtain standard solutions at 10 ppm, 25 ppm, 50 ppm, 75 ppm, 100 ppm, 125 ppm, and 150 ppm in 0.1 M acetate buffer, pH 4.5. A 1000 ppm master solution is prepared by carefully weighing 3.81 g of Cu(NO3) 2 · 3H2O, dissolving it in double-distilled water, and diluting to 1 L. Next, dilutions are performed to obtain standard solutions at 10 ppm, 25 ppm, 50 ppm, 75 ppm, 100 ppm, 125 ppm, and 150 ppm in 0.1 M acetate buffer, pH 4.5. All solutions are prepared using double water distillation (WaterOne).

2.8 Sample preparation and analysis

The sample used in this study is an artificial sample, where a Cd sample is made by adding a standard Cd solution at 10–125 ppm in an acetate buffer (0.1 M, pH 4.5) to the river water and the concentration of Cd is measured by cyclic voltammetry using SPCE/AgNPs-Chi and Atomic Absorption Spectrophotometer (AAS), to compare the measurement results and determine the accuracy of the Cd sensor.

3.Results and Discussion

3.1 Synthesis of AgNPs-Chi

AgNPs-Chi were successfully synthesized using a water extract of red ginger leaves, with silver nitrate solution as a precursor and chitosan as a surface-capping agent to prevent agglomeration [52]. AgNO3 dissociates in water to produce Ag+. The bioactive compounds identified in the phytochemical screening results showed that red ginger leaf extract contains flavonoids, tannins, steroids, and saponins [53], which play a role in reducing Ag+ ions to Ag0. Some previous studies have also reported that bioactive compounds in plants may act as degrading agents in the formation of silver nanoparticles [54-59]. Bioactive compounds from red ginger leaf water extract that have -OH groups, such as flavonoids, tannins, steroids, and saponins, undergo oxidation by releasing electrons, reducing the Ag+ in a 1 mM AgNO3 solution to Ag0. In addition to being a reducing agent, the bioactive compounds in red ginger leaf extract, such as phenolic compounds, flavonoids, tannins, steroids, and saponins, act as a capping agent, maintaining the stability of the silver nanoparticles formed [60-63]. In addition to secondary metabolites such as phenolics, terpenoids, and flavonoids, biomolecules with functional groups of aldehydes, carboxylic acids, and amides also act as reducing and stabilizing substances for nanoparticles [64]. The successful formation of silver nanoparticles is indicated by a color change from yellow to brownish-yellow. This discoloration has also been confirmed in previous research on the biosynthesis of chitosan-coated silver nanoparticles [65, 66, 67, 68, 69]. **Fig. 3** shows the discoloration of AgNPs-Chi over 7 days. According to [70], the color intensity of the AgNPs solution mixture increases over time. The color change in AgNPs-Chi indicates the excitation of surface plasmon vibrations in the formed silver nanoparticles [71]. The SPR phenomenon of AgNPs-Chi is further characterized using a UV-Vis Spectrophotometer.

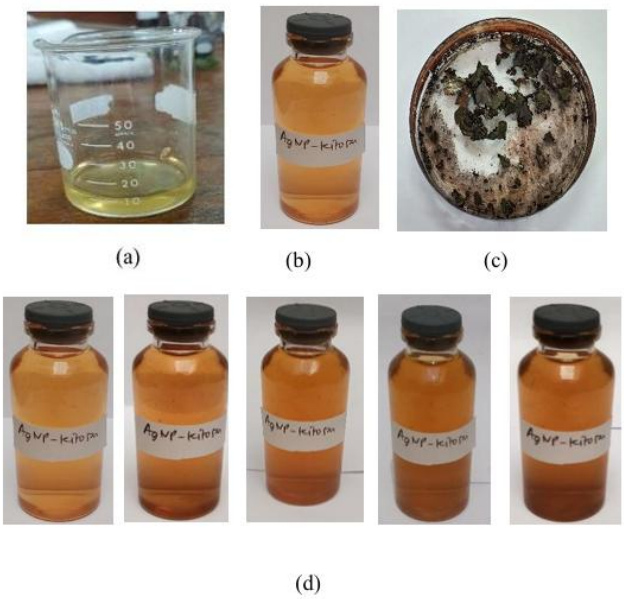


Fig 3. Figure (a) Red ginger leaf extract; (b) AgNPs-Chi Solution; (c) Dry AgNPs-Chi (d) Discoloration of AgNPs-Chi for 7 Days (Days 1 to 7, consecutively)

3.2 Characterization of AgNPs-Chi with UV-Vis Spectrophotometer

The bioactive compounds contained in red ginger leaves play an important role in the formation of AgNPs-Chi. During the seven-day period, from the first to the seventh day, AgNPs-Chi changed from yellow to brownish-yellow, indicating the successful synthesis of AgNPs-Chi. [72] confirmed that compounds from plant extracts used in the biosynthesis process can cause discoloration in silver nanoparticles. This color change is caused by the SPR (Surface Plasmon Resonance) effect, which can be verified with a UV-Vis spectrophotometer. Color change in the 1-7 day range began on day 2, but on days 3 -7, no color change was detected. This is one of the indicators of the stability of the AgNPs produced by Chi. According to [69], brownish color is caused by the excitation of free electrons in nanoparticles. After 24 hours, no further discoloration was observed, indicating that the synthesized nanoparticles had stabilized. In this study, red ginger leaf water extract contributed significantly to the formation of AgNPs-Chi. **Fig. 4** shows the AgNPs-Chi spectrum in a time span of 1 to 7 days, where the peak of UV-Vis absorption is at wavelengths of 432.5 – 452.5 nm. Wavelength and absorbance data for red ginger leaf extract and AgNPs-Chi over 1 to 7 days are shown in **Table 1**.

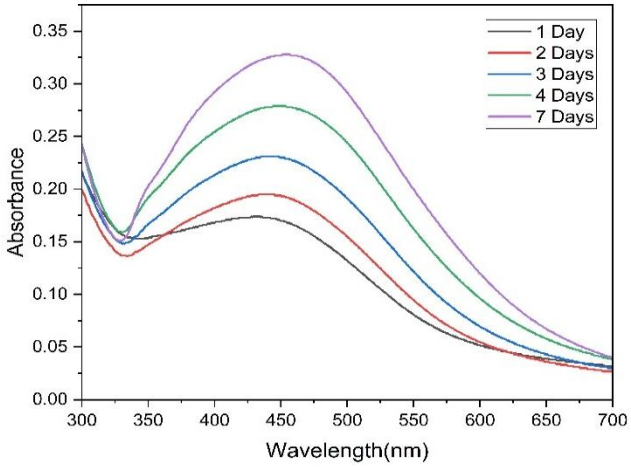


Fig 4. UV Vis AgNPs-Chi spectrum in a time range of 1 to 7 days

The sharp peak of AgNPs-Chi in the wavelength region of 432.5 - 452.5 nm is similar to previous studies where the peak of AgNPs-Chi nanocomposites is in the range of 400-460 nm [52, 66, 70, 73,74].

Table 1. UV-Vis absorption data of AgNPs-Chi

Time (days)	λ_{Max} (nm)	Absorbansi
1	432.50	0.174
2	440.00	0.195
3	442.00	0.231
4	447.50	0.279
7	452.50	0.328

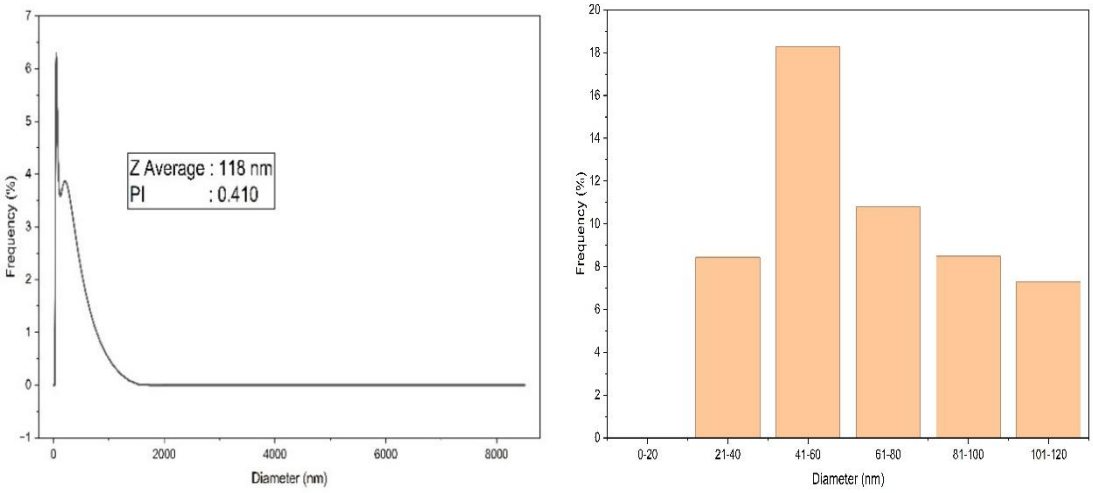
Table 1 shows the increase in absorbance over time for AgNPs-Chi. Previous research has shown that the peak absorption strength increases over time [75]. The absorbance of AgNPs-Chi increased from 0.174 on the first day to 0.328 on the seventh day, indicating an increase in the number of nanoparticles formed during the synthesis process. The results obtained are in line with previous research, which suggested that the formation of silver nanoparticles is influenced by the reduction of Ag+ ions to Ag0. The longer the biosynthesis process lasts, the more silver nanoparticles are formed, as evidenced by increased absorbance [76]. Red ginger leaf extract can enhance the increased absorbance and stability observed during AgNP formation. The higher the amount of bioactive compounds contained in the extract, the more stable the size of the silver nanoparticles produced will be [77]. The biosynthesis process on the first day shows that only a small amount of Ag+ is reduced to Ag0. The next day, a significant increase in absorbance is observed for the silver nanoparticles until Ag+ is completely reduced to Ag0. UV-Vis Surface Plasmon Resonance (SPR) is highly sensitive to the dimensions and morphology of silver nanoparticles [72]. The spherical shape of silver nanoparticles is characterized by a single SPR band in the 300-700 nm range [78].

In this study, the stability of AgNPs-Chi is influenced not only by the bioactive compound content in leaf extracts but also by the presence of chitosan. Chitosan was used in this study to improve its stability and functionality. According to [79], AgNPs that have been modified in the formation of metal nanoparticles will be affected by the presence of capping agents. The capping agent itself is a substance that can stabilize silver nanoparticles that have been previously synthesized by their aggregation. There are various types of capping agents, including chitosan. Chitosan acts as a steric barrier by covering the metal surface with a positive charge. Chitosan is used as a surface stabilizer for silver nanoparticles to prevent agglomeration, as naked metal nanoparticles tend to clump due to van der Waals interactions [72]. [80] stated that chitosan is an excellent stabilizing agent for metal nanoparticles. In addition to serving as a stabilizer, chitosan in this study was used to modify the surface of nanoparticles, thereby facilitating the functionalization of AgNPs-Chi in cadmium and copper metal sensors.

3.3 Characterization of AgNPs-Chi with PSA

Characterization of AgNPs-Chi was followed by PSA to determine the nanoparticles' mean overall diameter. Particle size is measured by dynamic light scattering, in which the motion of particles in the medium is correlated with their size [81]. The results of the AgNPs-Chi size distribution test using PSA are shown in **Fig 5,** shows the average particle size and size distribution in AgNPs-Chi. The results showed that the average size of AgNPs-Chi particles was 118 nm, with a polydispersity index (PI) of 0.410. This indicates that the average particle size of AgNPs-Chi is well distributed, where if the PI value is closer to zero (0), the size distribution and physical stability of silver nanoparticles are better [82]. The PI value can also provide an overview of nanoparticle size homogeneity in solution, with larger PI values indicating less uniform nanoparticle size [83]. The PI value in this study was lower than that in the previous study by

[84], which reported a PI value of AgNPs/Chi of 0.6.



(a) (b)

Fig 5. (a). Average size of AgNPs-Chi (b). AgNPs-Chi size distribution

The average size of AgNPs-Chi obtained was 118 nm, larger than the size of AgNPs, which was 53.6 nm (**Fig. 5a**). These results show an increase in the average size of the nanoparticles after being modified with chitosan, as the chitosan layer covers the silver nanoparticles [85], proving that the nanoparticle modification process has been successfully carried out. This is in line with previous research by [66, 67, 69, 86], who used the DLS technique and reported an increase in the mean size of AgNPs-Chi after chitosan modification. **Fig. 5b** shows the histogram of the particle size distribution in AgNPs-Chi, where the most dominant distribution is seen at the size of 41-60 nm with an intensity of 18.3%. The particle size distribution of AgNPs-Chi varies from 31.01 to 118.74 nm. Silver nanoparticles coated by chitosan have a wide size distribution due to the size of the chitosan molecule and the number of chitosan layers on the nanoparticle's surface [52].

3.4 Characterization of Chitosan Modified Silver Nanoparticles with FTIR

FTIR analysis was carried out to determine the success of the AgNPs modification process using chitosan as a capping agent, which stabilizes nanoparticles, by analyzing the absorption spectrum and infrared emissions. The FTIR spectrum of AgNPs-Chi can be seen in **Fig. 6**. This spectrum shows several uptake peaks that indicate the presence of various functional groups involved in the synthesis of AgNPs-Chi. The dominant absorption peaks for AgNPs-Chi were observed at peaks of 3446.79, 2926.01, 2362.80, 1653, 1382.96, 1153.43, 1078.21, 1022.27, 858.32, 524.64 cm-1. The results of the functional group analysis of AgNPs-Chi from red ginger leaf water extract are shown in **Table 2**.

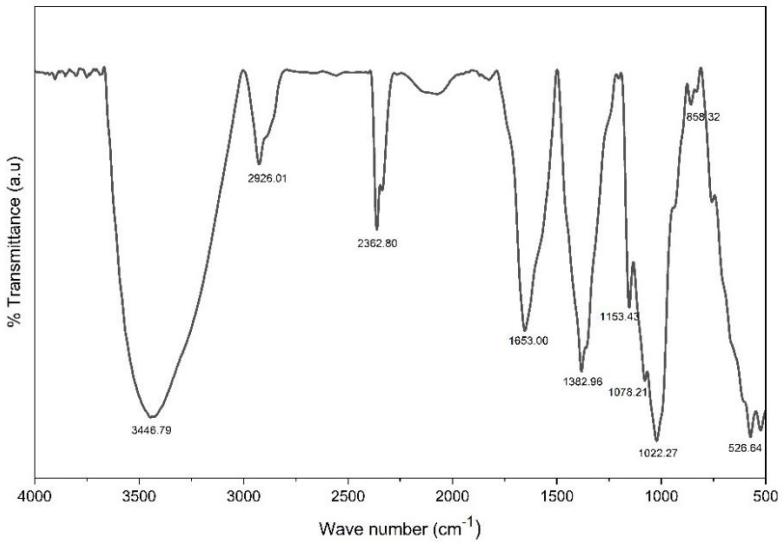


Fig 6. FTIR Spectrum AgNPs-Chi

Table 2. Results of AgNPs-Chi functional group analysis

No.	Number of Waves (cm^{-1}) AgNPs	Description of functional groups
1.	3446.79	OH and NH stretch vibration
2.	2926.01	CH stretch vibration
3.	2362.80	Stretch vibration O=C=O
4.	1653.00	Stretch vibration C=O (amide I)
5.	1382.96	C-N stretch vibration
6.	1153.43	Stretching vibration C-O-C (glycosidic bond)
7.	1078.21	C-O stretch vibration
8.	1022.27	C-O stretch vibration
9.	858.32	Aromatic C=CH stretch vibration
10.	524.64	Ag-O stretch vibration

The results of the FTIR analysis showed a band at 3446.79 cm^{-1} is associated with overlapping N-H stretches of O-H stretches of carbohydrate rings as well as intramolecular hydrogen bonds [67, 68, 69, 74]. Absorption tape at 2926.01 cm^{-1} conforms to the symmetrical stretch of C-H [74]. Pie falls 2362.80 cm^{-1} considered as a stretch O=C=O (CO2) absorbed from the atmosphere [87]. Tape at 1653.00 cm^{-1} can be attributed with amide vibration characteristic I due to the presence of stretch vibration C=O [74]. Number of waves 1382.96 cm^{-1} indicates C-N stretching vibrations signaling the presence of secondary amine groups and chitosan structures [88]. Absorption tape at 1153.43 cm^{-1} ; 1078.21 and 1022.27 cm^{-1} can be attributed to the C-O-C (glycosidic bond) stretch vibration and C-O stretch of the carbohydrate ring [69, 89, 90]. In addition, there is a ribbon at 1653 – 1022 cm^{-1} according to the C=O stretch vibration, C-N stretch, and CH_3 and C-O-C bending vibtrations, indicating the presence of a carbohydrate structure [91, 92]. AgNPs-Chi displays two bands at 1022.27 and 1078.21 cm^{-1} [66]. These bands are associated with C-O-C and C-O stretching vibrations in chitosha-like polysaccharides [69]. The existence of these two distinct peaks compared to the single bands in AgNPs-Chi provides evidence of successful integration of chitosan to the surface of nanoparticles [93]. These chemical

modifications reflect the formation of chitosan nanoparticle interfaces [94]. According to [95], the absorption bands between 1000 - 1100 cm^{-1} serve as a reliable indicator of the presence of chitosan on the surface of AgNPs, reinforcing its role in improving the stability and dispersion of nanoparticles in polymer matrices.

The absorption band at 858.32 cm^{-1} showed the presence of aromatic C=CH vibrations [96] and confirmed the structure of chitosan polysaccharides, consistent with findings by [97], who identified CH deformation bands as markers of polysaccharides-nanoparticle interactions. The band at 524.64 cm^{-1} indicates the occurrence of Ag-O stretch vibrations and indicates the formation of AgNP-Chi which occurs in wavenumbers of 400 – 700 cm^{-1} [73, 98]. Based on these results, it can be seen that there is a shift in the number of waves in AgNPs-Chi which indicates an interaction between the functional groups found in AgNPs and chitosan [84]. In addition, the observed peaks of N-H and C-O confirm the contribution of chitosan, suggesting that the chitosan layer not only improves stability but can also facilitate the further functionalization of AgNPs [68].

3.5 Characterization of AgNPs-Chi with XRD

The crystallinity and size of AgNPs-Chi were analyzed using XRD. XRD analysis also confirmed the crystallite arrangement of the formed AgNPs-Chi. The results of the analysis of XRD AgNPs-Chi can be seen in **Fig. 7.** The peaks of the AgNPs-Chi diffraction pattern are at 37.817°, 44.063°, 64.434°, and 77.539°, corresponding to the crystallite lattice planes (111), (200), (220), and (311). This reflects the typical pattern of silver with a face-centered cubic crystallite structure, according to the Joint Committee on Powder Diffraction Standards (JCPDS) database number 04-0783 [75]. These results are in line with previous research [68, 99, 100, 101]. In addition, some weak peaks were observed on the diphroctograms, which may have originated from the formation of bioorganic compounds on the surface of silver nanoparticles. This also occurs during the formation of silver nanoparticles, as reported by other researchers [102, 103].

The XRD pattern in AgNPs-Chi has similar characteristics to the XRD pattern, suggesting that AgNPs-Chi effectively combines AgNPs and shares a similar structural configuration, confirming the successful synthesis of AgNPs-Chi [68]. According to [69], the incorporation of chitosan around the nanoparticles does not alter the XRD pattern of AgNPs, which shows the same peak, indicating that the chitosan layer does not alter the nanoparticles' crystallinity or structure [69]. All of the diffraction peaks in **Fig. 7** exhibit characteristics of AgNPs-Chi as a crystalline structure, with slight shifts in peak positions due to strain [104]. The presence of sharp, well-defined diffraction peaks emphasizes the high purity and crystallinity of AgNPs-Chi [68]. In the diffraction pattern of AgNPs, there are additional peaks that may be caused by phytochemical constituents of plant extracts used in the synthesis of AgNPs [105] and the presence of peak expansion due to the amorphous properties of chitosan polymers [106,107].

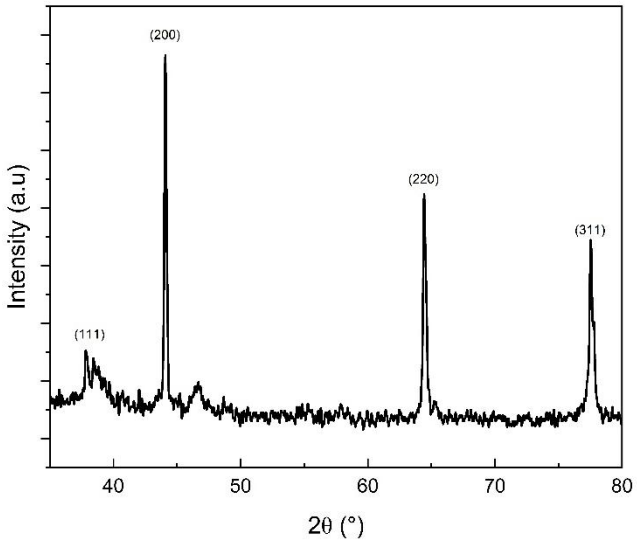


Fig. 7. AgNPs-Chi XRD diffraction pattern

The lattice plane (200) in AgNPs-Chi is a parallel plane that divides the cubic structure horizontally. Peaks in the AgNPs-Chi diffraction pattern in the field (200) show higher intensity than other lattice planes, indicating that although there are crystallites oriented to the lattice plane (111), (220), and (311), the majority of crystallite structures tend to be more oriented to the plane orientation (200) [108]. The level of crystallinity of a nanoparticle is indicated by the peak intensity of diffraction and the FWHM (Full Width Half Maximum) value. Nanoparticles with high diffraction peak intensity and low FWHM values exhibit high crystallinity [109, 110]. AgNPs-Chi has a peak with high intensity and a small FWHM value, indicating that AgNPs-Chi has a high level of crystallinity. However, in the lattice planes 111, 220, and 311, the peak intensity of AgNPs-Chi diffraction decreases because the AgNPs surface is covered with chitosan during the modification process. The diffraction peaks of AgNPs-Chi tend to be sharper than the diffraction peaks of AgNPs, indicating that the crystallite size of AgNPs-Chi is greater than the crystallite size of AgNPs. According to [111], sharper diffraction peaks indicate a larger crystallite size. The crystallite size of AgNPs-Chi was determined using the Debye-Scherrer equation [112] (Equation 1). The value of K is the constant of the material, which is 0.9, λ is the wavelength of the X-ray (1.54 Å), and β is the value of FWHM. The calculation results obtained that the average crystallite size of AgNPs-Chi is 61.98 nm. Meanwhile, the calculated lattice parameters for silver nanoparticles averaged 0.409 nm. The lattice parameter values obtained are close to the lattice values of silver nanoparticles based on JCPDS No. 04-0783 (a= 0.407 nm).

Table 3. Average size of AgNPs-Chi crystallites

$2D\ (^{O})$	HKL	FWHM	D (nm)	Crystallite Size (nm)	Parameter kisi (a) (nm)
37.817	111	0.11330	0.2377	80.67	0.412
44.063	200	0.14960	0.2053	62.35	0.411
64.434	220	0.19690	0.1444	51.91	0.408
77.539	311	0.20930	0.1230	52.99	0.408
Average size:			0.1776	61.98	0.409

3.5 Characterization of AgNPs-Chi with SEM-EDX

The surface morphology of AgNPs-Chi was analyzed using the SEM-EDX (Scanning Electron Microscope-Energy Dispersive X-Ray Spectroscopy) method. SEM-EDX is a combination of two methods: SEM, which determines the morphology of a solid sample from images, and EDX, which analyzes the chemical elements of a material [113]. The SEM method can be used to scan nanoscopic structures at high resolution [114]. The EDX method validates the elemental composition of the synthesized AgNPs-Chi [67]. The measurement begins with SEM to obtain a morphological image of the silver nanoparticles at 5000x magnification, with a scale of 10 μm, as shown in **Fig. 8.**

SEM analysis showed the surface morphology of AgNPs-Chi. **Fig. 8** shows silver nanoparticles enveloped by chitosan polymers [84, 115, 116] and occupying spaces between nanoparticles [84]. In general, **Fig. 8** shows aggregated AgNPs-Chi that appear clumped. Aggregation of silver nanoparticles occurs due to their high surface energy and reactivity, which causes them to attract one another and form clusters [117, 118]. **Fig. 8** also confirms that AgNPs-Chi are spherical and randomly dispersed. Similar findings have also been reported by [67, 68, 69, 84, 116, 119].

The AgNPs-Chi micrograph also shows a more uniform, homogeneous surface. This uniformity in size and distribution is likely due to the stabilizing effects of chitosan, which forms a protective layer around AgNPs, reducing their tendency to aggregate. The chitosan layer not only increases nanoparticle size but also enhances stability and dispersion [68]. [69] reported the results of SEM AgNPs-Chi, synthesized from wheat residues, showing lower nanoparticle aggregation, possibly due to chitosan stabilization on the nanoparticle surface, resulting in repulsion between nanoparticles due to the positive

surface charge of the nanoparticles. In another study, the use of chitosan as a coating agent for other metal nanoparticles, such as gold, improved stability compared to gold nanoparticles without chitosan [120].

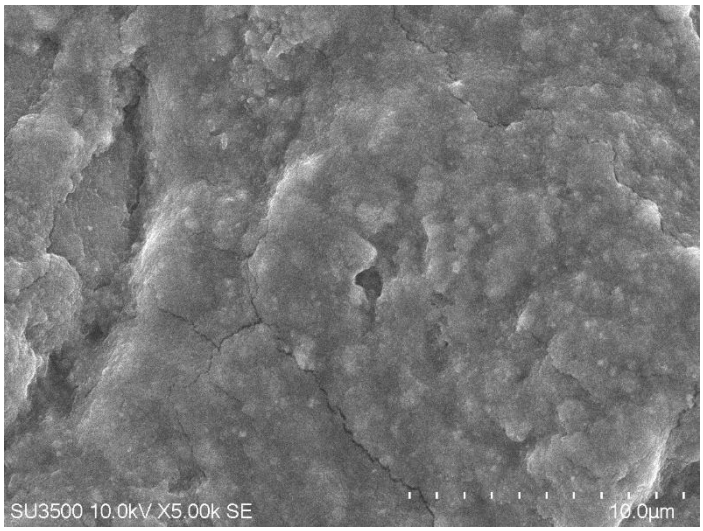


Fig. 8. Surface morphology of AgNPs-Chi with SEM magnification of 5000x at scale of 10 µm

The next measurement is by Energy-Dispersive X-Ray Spectroscopy (EDX), which aims to characterize AgNPs-Chi based on their elemental content. The spots or dots identified by EDX measurements reveal the specific chemical composition of the silver nanoparticles. The results of EDX measurements of the chemical composition of silver nanoparticles are shown in Fig. **9**.

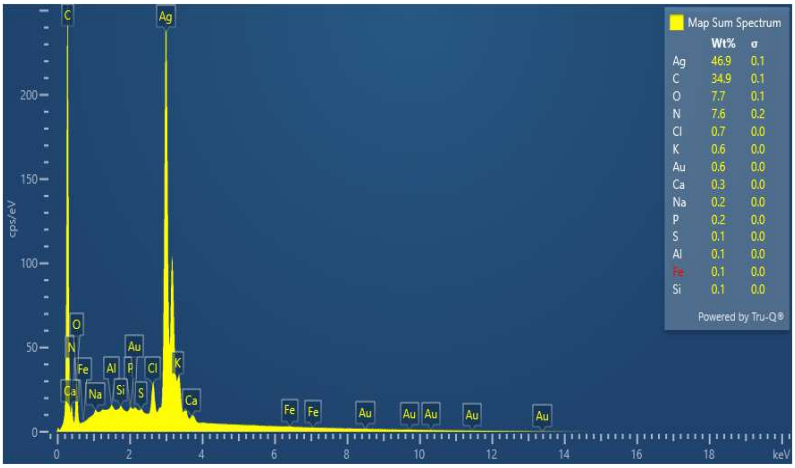


Fig. 9. EDX spectrum on AgNPs-Chi

The EDX spectrum of AgNPs-Chi shows that silver is the dominant element, with a 3 keV peak. Previous research has also shown that silver is near a peak at 3 keV [65, 67, 69]. The composition of Ag 46.9%, C 34.9%, O 7.7%, and N 7.6% indicates that silver is the main component of AgNPs-Chi, confirming the successful synthesis of AgNPs-Chi and the successful modification of chitosan with silver nanoparticles. These findings are in line with [121], who also reported the presence of C and O in AgNPs/chitosan mediated by Mentha piperita. According to [74], the presence of C and O along with Ag indicates the presence of chitosan on the surface of the silver metal. The C peak corresponds to the organic chitosan structure, while the O and N peaks are related to the chitosan structure and surface oxidation of silver nanoparticles [68]. The spectrum also indicates the presence of several other elements, including Cl, K, Au, Ca, Na, P, S, Al, Fe, and Si. The detection of additional elements other than Ag is due to the release

of compound components from leaf extracts via X-rays [122] and to the chitosan composition [67]. This suggests that red ginger leaf extract has a dual role as a reducing and stabilizing agent during nanoparticle synthesis, enhancing the biocompatibility and functional diversity of AgNPs-Chi [67].

3.**Results and Discussion**

4.1 Electrochemical measurements using SPCE/AgNPs-Chi as Cd and Cu metal sensors

The CV response to SPCE/AgNPs-Chi and SPCE can be seen in **Fig. 10**. CV measurements were performed in a 0.1 M acetate buffer solution, pH 4.5, with a scan rate of 50 mV/s, in a potential range of +1 V to -1 V for Cu metals, showing a higher current response in SPCE/AgNPs-Chi compared to SPCE. This increase in electrochemical peak current suggests that AgNPs-Chi has good electrical conductivity, more active sites, and excellent electrocatalytic activity [123, 124, 125]. This is in line with previous research by [123], which found that diizhone-chitosan-modified AgNPs exhibit good electronic properties, including rapid electron transfer at the SPE surface, leading to increased current and sensitivity for electrochemical detection of [Fe(CN)6]3-/4-. Research conducted by [126] also showed an increase in current peaks in GCE/AgNPs-chitosan electrodes compared to GCE electrodes for lipopolysaccharide analysis. This suggests that the presence of AgNPs-Chi with an active surface bearing -NH2 [127] as a capping agent can increase electron transport at the electrode surface, increase peak current, and result in stronger sensor interactions [124].

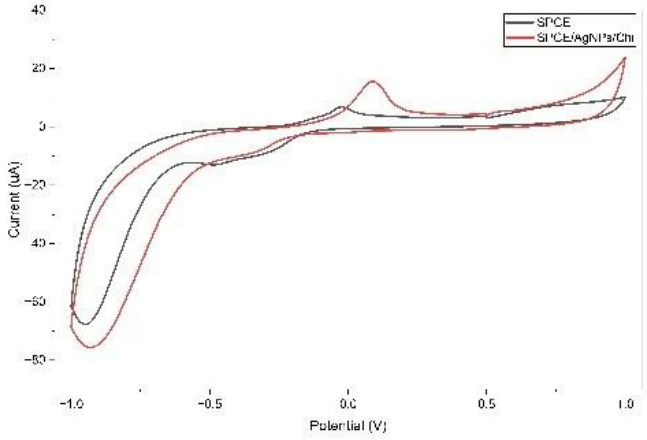


Fig. 10. CV SPCE/AgNPs-Chi response at scan rate 50 mV/s in a 0.1 M acetate buffer solution pH 4.5

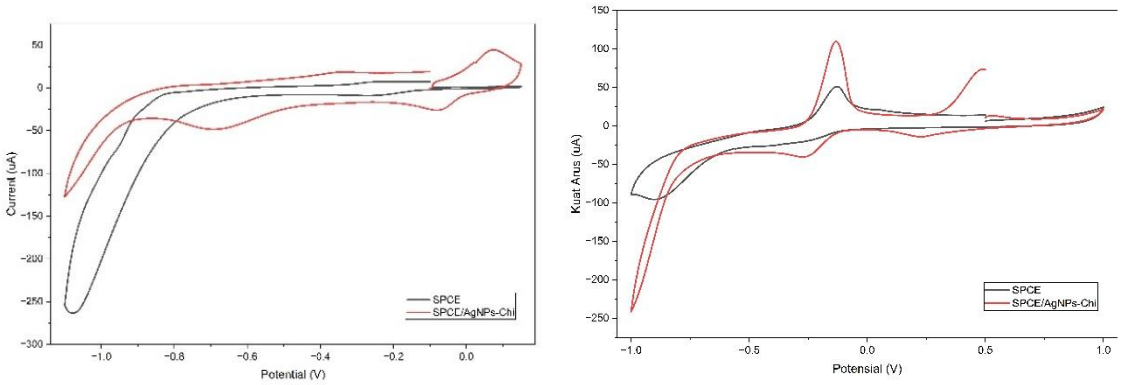
The SPCE anodic peak is observed at a current of 6.79 µA, while the SPCE/AgNPs-Chi peak is observed at a current of 15.58 µA. The presence of this anodic peak is thought to result from silver oxidation, as shown in **Fig. 10**. Under acidic/neutral pH conditions, such as in a pH 4.5 acetate buffer, silver undergoes anodic oxidation to Ag^+. The Ag^+ ions formed then complex with the acetate anion to become $Ag(CH_3COO)$ [128,129,130,131]. The reaction of silver ions in the acetate buffer at pH 4.5 is shown in Fig. **11**.

$$Ag_{(s)} \rightarrow Ag^+_{(aq)} + e^-$$

$$Ag^+_{(aq)} + CH_3COO^-_{(aq)} \rightleftharpoons Ag(CH_3COO)_{(aq)}$$

Fig. 11. Silver ion reaction in acetate buffer pH 4.5

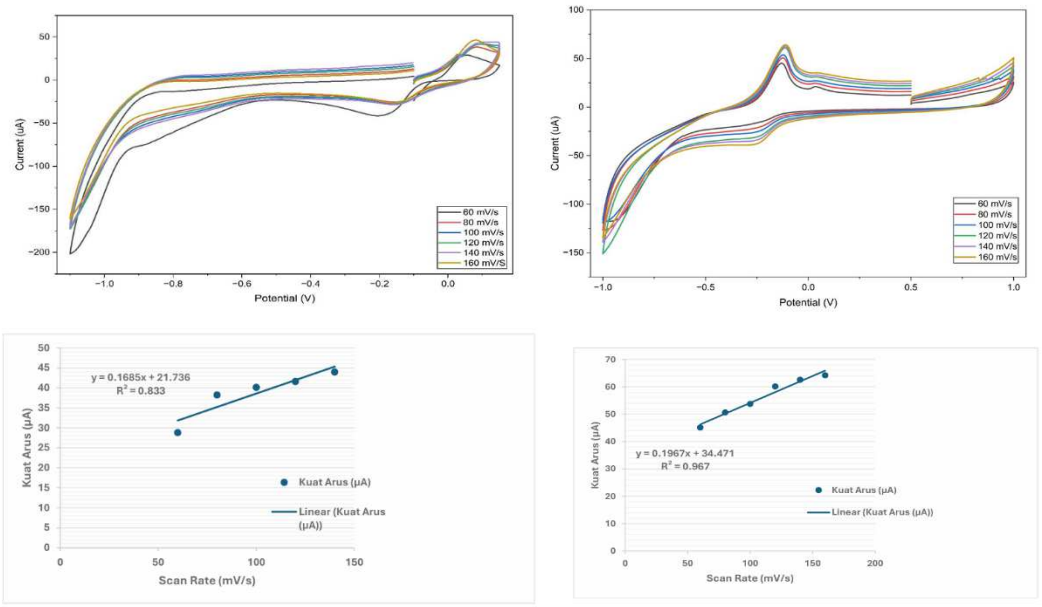
Fig. 12 shows the CV response of SPCE and SPCE/AgNPs-Chi electrodes to a 125 ppm Cd and Cu metal solution with a scan rate of 50 mV/s. **Figure 12(a)** shows the response of the SPCE electrode to a 125 ppm Cd metal with a very weak oxidation peak intensity with a current of 1.19 µA, while the SPCE/AgNPs-Chi electrode shows a very sharp peak with a current of 44.77 µA. **Figure 12(b)** shows the response of the SPCE electrode to a 125 ppm Cu metal with an intensity of 1.19 µA. lower oxidation peak at SPCE (current 51.07 µA), while SPCE/AgNPs-Chi electrodes show very high oxidation peak at 109.6 µA.



(a) (b)

Fig. 12. CV SPCE/AgNPs-Chi response at a scan rate of 50 mV/s in a solution of (a) Cd 125 ppm (b) Cu 125 ppm

The effect of scan rate on SPCE/AgNPs-Chi was determined using CV at a scan rate of 60 -160 mV/s with an interval of 20 mV/s in a Cd and Cu solution of 125 ppm, as shown in **Fig.13**, which shows the peak of oxidation that shifts in a positive direction with an increase in the scan rate. The results of these observations indicate that the reaction of Cd and Cu with the SPCE/AgNPs-Chi electrode surface follows a controlled diffusion process. This is in line with previous research by [132], which showed a linear increase in peak current [Fe(CN)6]3-/4- at the SPE and SPE-AgNPs-Dtz@Cts electrodes with increasing scan rate. According to [133, 134], the current peak is directly proportional to the scan rate when the measurement parameters remain constant. Fig. 12 also shows the correlation between the peak current (µA) and the square root of the scan rate (mV/s)1/2 on the SPCE/AgNPs-Chi electrode. Based on **Fig. 13**, a linear relationship between the peak current (µA) and the square root of the scan rate (mV/s)1/2 is observed. This indicates that the reaction rate at the electrode surface is influenced by the rate of electron transfer on the silver-chitosan nanoparticle-modified electrode. The linear plot shows that the SPCE/AgNPs-Chi-modified electrode yields R2 values of 0.833 for Cd and 0.967 for Cu.



(a) (b)

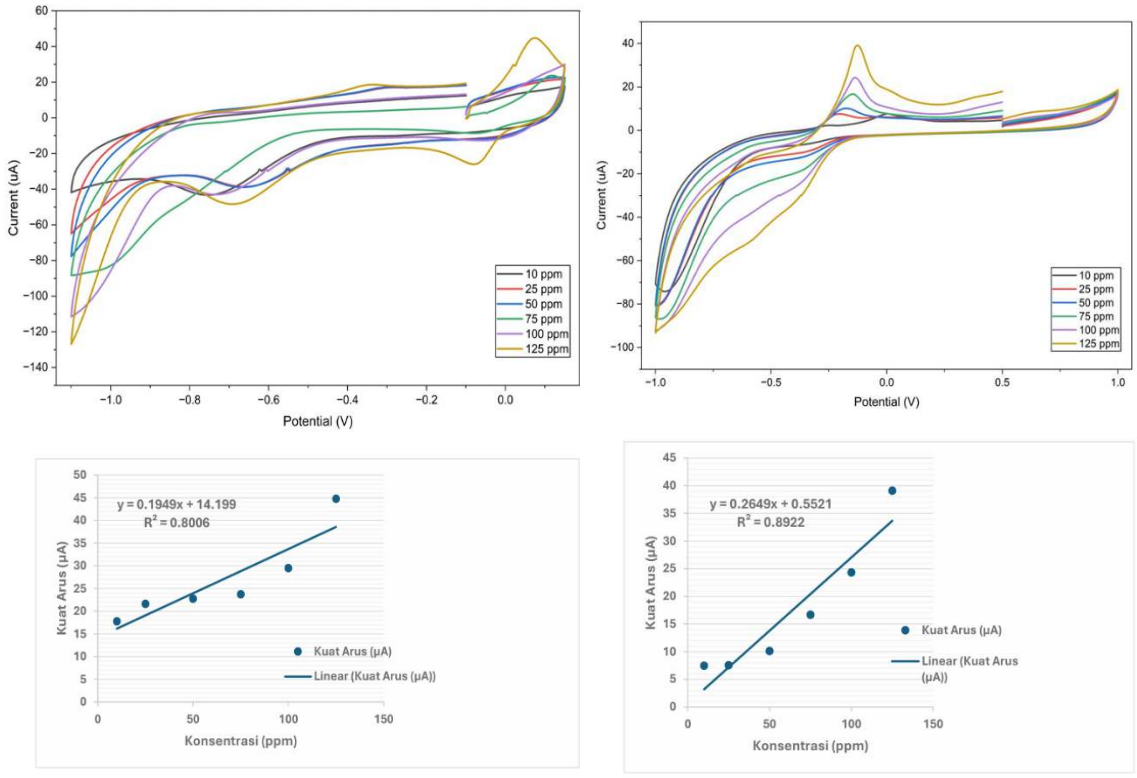
Fig. 13. CV response and linear plot of SPCE/AgNPs-Chi with a scan rate of 60-160 mV/s in a Cd solution of 125 ppm; (b) Cu 125 ppm

The sensor response of the SPCE/AgNPs-Chi modified electrode was evaluated at various concentrations of Cd (10-150 ppm) and Cu (10-125 ppm) at a scan rate of 50 mV/s. **Fig.14** shows the CV response and linear plot of the SPCE/AgNPs-Chi electrode. The increase in current can be seen as there is an increase in the concentration of Cd **(Fig. 14a)** and Cu (**Fig. 14b**). The current at the resulting anodic peak is directly proportional to the concentration of the standard Cd and Cu solutions achieved and results from the transfer of electrons moving from the sample (metal solution) to the electrode surface [125]. This is in line with research by [132], which shows that current increases along with Hg2+ concentration at the SPEs-AgNPs/Dithizone/chitosan electrodes. Current changes in response to increased concentrations of Cd and Cu can be attributed to strong electrostatic interactions between AgNPs-Chi and Cd and Cu [126]. The resulting linear plot shows a linear relationship in the metal concentration range of Cd 10-125 ppm, resulting in a linear regression equation $y = 0.1949x + 14.199$ ($R^2 = 0.8006$). Meanwhile, the linear plot in the Cu concentration range of 10-125 ppm yields the equation $y = 0.2649x + 0.5521$ ($R^2 = 0.8922$). Data on concentration, current strength, and response time in SPCE/AgNPs-Chi are shown in **Table 4**.

Table 4. Data concentration, current strength, response time on SPCE/AgNPs-Chi

Concentration (ppm)	Current strength (µA)		Response Time(s)	
	Metal Cd	Cu Metal	Metal Cd	Cu Metal
10 ppm	17.8025	7.475	7.0	35.8
25 ppm	21.6396	7.5583	6.5	36.0
50 ppm	22.7546	10.1167	6.0	36.4
75 ppm	23.7525	16.6958	5.3	37.8
100 ppm	29.5133	24.3375	4.8	38.5
125 ppm	44.7750	39.1167	4.8	38.7
Measurement Range	1 – 125 ppm	1 – 125 ppm		
R2	0.8006	0.8922		
Pers. Reg. Linier	y = 0.1949x + 14.199	y = 0.2649x + 0.5521		
Time range			4.8 – 7.0	36.0 – 38.7

In this study, the response time of SPCE/AgNPs-Chi was determined to assess the electrode's sensitivity; the shorter the response time, the greater the electrode's sensitivity [135]. Table 4 shows SPCE/AgNPs-Chi response time data at a scan rate of 50 mV/s, where the response time for Cd metal analysis ranges from 4.8 to 7.0 s, while the response time for Cu analysis ranges from 36.0 to 38.7 s. The current response time to the concentration of Cd is shorter than that of Cu.



(a) (b)

Fig. 14. (a). CV response and linear plot SPCE/AgNPs-Chi at a scan rate of 50 mV/s for (a) Cd solution 10 -125 ppm, (b) Cu solution 10 - 125 ppm

The detection limits and sensitivity of the modified electrodes are also determined. The following equation [136] was used to determine LOD in this study: LOD = 3 SD/s, where SD is the standard deviation of the empty peak current (six runs), SD = 0.6156, and s is the slope of the corresponding calibration equation. The detection limit is calculated from the empty solution (electrolyte) and the standard curve relating metal concentration to electrode current. The results of the calculation of the detection limit (LoD) of Cd metal using the SPCE/AgNPs-Chi electrode obtained a value of 9.48 ppm (0.08 mM). Meanwhile, the results of the calculation of the Cu detection limit using the SPCE/AgNPs-Chi electrode obtained a value of 6.97 ppm (0.11 mM). The results of the calculation of the quantification limit (LoQ) of Cd using the SPCE/AgNPs-Chi electrode obtained a value of 31.59 ppm (0.08 mM). Based on the results, the SPCE/AgNPs-Chi electrode can detect Cd metal at 9.48 ppm (0.08 mM) and Cu metal at 6.97 ppm (0.11 mM).

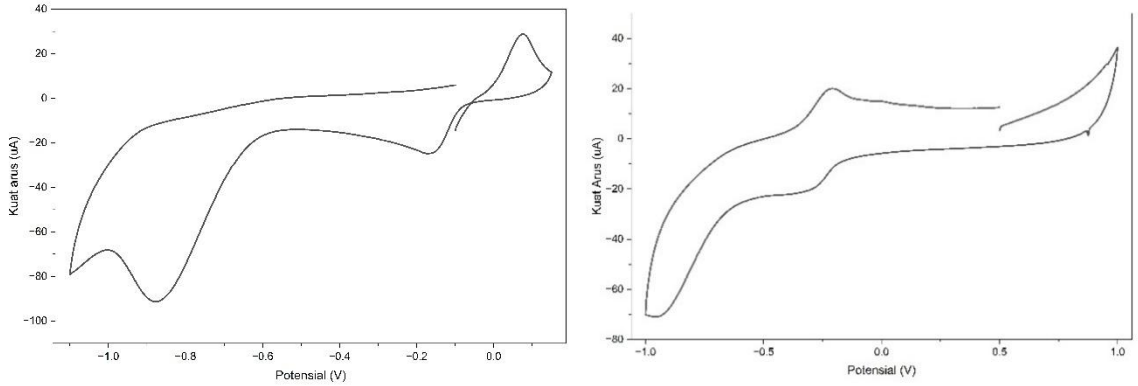
The high LOD in this analysis suggests that the sensor cannot produce sufficiently distinct signals from noise at trace levels, making its performance less than ideal for trace analysis applications [137], which can be due to several factors, including the fact that CVs are less sensitive to heavy metal detection at very low levels, compared to stripping techniques such as ASV or SWASV. The detection limit (LoD) for Cd and Cu analysis by cyclic voltammetry is generally high due to the CV's low intrinsic sensitivity, especially at trace concentrations. CV does not include the preconcentration stage, so the redox current is small and can be easily covered by capacitive currents [138]. In SPCE/AgNPs-Chi, the peak current produced is relatively small, especially in Cd, making it difficult to distinguish the analyte signal from the noise. Low currents can result from less efficient electron transfer at the electrode surface, a limited active surface area, or electrode modifications that do not form optimal active sites [139]. When the signal flow is low, the difference between the signal and baseline becomes small, which ultimately increases the LoD.

Additionally, high base noise is another significant factor contributing to the increase in LoD [140]. Factors such as electrode surface fouling by sample matrix components, voltammogram baseline instability, and interference from other compounds may also contribute to increased signal variation [138]. Low sensitivity also contributes to high LoD values. The low sensitivity is reflected in the slight tilt of the calibration curve, suggesting that changes in analyte concentration result only in subtle changes in current [141]. In addition, the potential for fouling by biomolecules or organic compounds can compromise electrode performance. Fouling can inhibit the analyte's access to the electrode surface, leading to decreased current and increased signal variability [142]. Therefore, although the electrode can measure metals at moderate concentrations, its performance is not yet ideal for trace-level applications and requires further optimization, such as improving surface modifications or using more sensitive stripping voltammetry techniques. Sensitivity is determined by dividing the slope of the linearity curve by the working electrode surface area used [81]. Sensitivity tests are conducted to assess a sensor's response to analytics. The SPCE/AgNPs-Chi electrode sensitivity test result for Cd metal analysis was 0.25 μAppm-1 mm-2. Meanwhile, the sensitivity of the SPCE/AgNPs-Chi electrode for Cu metal analysis was 0.34 μAppm-1mm-2. These results show that the SPCE/AgNPs-Chi electrode is more sensitive to Cu than to Cd.

The electrode's sensitivity is inversely proportional to the particle size. The smaller the particle size (up to the optimal size), the higher the electrode's sensitivity [143]. AgNP is a nanoscale particle with a larger active surface area, allowing the adsorption of more metal ions (Cd2+/Cu2+) and providing a more active site for reactions, resulting in a linear increase in peak current and high sensitivity [143] [144,145,146]. In addition, with a large surface area, AgNPs can facilitate the oxidation of electroactive species at electrodes by increasing mass transport rates and enabling rapid electron transfer, thereby enhancing electrode sensitivity [143] [145] [147,148].

4.2 Simultaneous Determination of Cd and Cu

Testing of artificial samples was also conducted to assess the ability of electrodes modified with SPCE/AgNPs-Chi silver nanoparticles to act as sensors for Cd and Cu. **Fig.15** shows the CV response of the SPCE/AgNPs-Chi electrode to the sample of an artificial metal solution in measuring the concentration of Cd and Cu. From the measurement results, the concentrations of Cd and Cu were 75.08 ppm and 73.5 ppm, respectively. The results of this measurement were compared with those of measurements using the Atomic Absorption Spectrophotometer (AAS), which yielded Cd concentrations of 50 ppm and Cu concentrations of 72.22 ppm. The measurement results using the SPCE/AgNPs-Chi electrode were close to those obtained with the Atomic Absorption Spectrophotometer (AAS) instrument, with analysis accuracies of 150.2% for Cd and 101.8% for Cu.



(a) (b)

Fig.15. CV SPCE/AgNPs-Chi response to artificial samples at a scan rate of 50 mV/s for (a) Cd (b) Cu
(b)

The results of this study show that the sensitivity and accuracy of Cu are better than those of Cd. This is due to the stronger affinity of the Cu complexion for amine groups and hydroxyl groups in chitosan, resulting in a larger peak current and a linear relationship with concentration. In addition, the slope of the calibration curve for Cu (0.1967) is greater than that for Cd (0.1685). Cu generally results in higher peak currents in voltammetric techniques because it exhibits faster electron-transfer kinetics and a tendency to interact more strongly with the surfaces of carbon-based electrodes or modified nanomaterials [149]. Such a high current response increases sensitivity. The presence of silver nanoparticles (AgNPs) accelerates the transfer kinetics of the Cu^{2+}/Cu^{0} redox reaction electrons compared to Cd^{2+}/Cd^{0}, resulting in a sharper and well-defined Cu voltammetry peak. The process of Cu deposition–dissolution during CV scanning is also more stable and homogeneous, whereas Cd tends to undergo partial redissolution or diffusion into the chitosan matrix, which decreases signal stability. Cu oxidation peaks appear at more positive potentials and are more separated from the background capacitive current, resulting in a higher signal-to-noise ratio, reduced measurement errors, and improved accuracy and sensitivity of Cu analysis compared to Cd [137, 138, 144, 146].

Conclusion

This study demonstrated the successful synthesis and characterization of chitosan-coated silver nanoparticles using a green, easy-to-follow, environmentally friendly, and cost-effective method that employs red ginger leaf extract as a coating agent and a natural reducing agent. Silver nanoparticles obtained by green synthesis (AgNPs-Chi) were used to modify SPCE for the simultaneous determination of Cd and Cu in an artificial metal solution by cyclic voltammetry. The results of UV-Vis, PSA, FTIR, XRD, and SEM-EDX spectroscopy confirmed the successful synthesis of AgNPs-RGL. The formation of AgNPs-Chi was visually confirmed by the discoloration and validated by UV-Vis analysis, which showed a surface plasmon resonance band at 432.5 nm, and was stable during the 7-day incubation period. The AgNPs-Chi particles analyzed by PSA have an average size of 118 nm and a well-distributed polydispersity index of 0.410. XRD and SEM-EDX analysis revealed the FCC-shaped AgNPs-Chi and identified silver as the dominant element, along with several other elements, including carbon, oxygen, and nitrogen. FTIR analysis confirmed the successful integration of chitosan to the surface of AgNPs, thereby stabilizing its dispersion in aqueous media. AgNPs-Chi has the potential to be developed as an SPCE modifier for the simultaneous determination of Cd and Cu by cyclic voltammetry, owing to its large surface area and higher catalytic activity, resulting in good performance. The SPCE/AgNPs-Chi analysis for Cu offers better sensitivity, detection limits, stability, and accuracy than Cd, with accuracy values 150.2% and 101.8% for Cu and Cd, respectively.

Acknowledgments

The authors would like to express their sincere gratitude to all parties who have contributed to this research. Their support and assistance are greatly appreciated

Authors Contribution

Rachmin Munadi : Writing – review & editing, Writing – original draft, Visualization, Resources, Project administration, Methodology, Investigation, Formal analysis, Data curation, Conceptualization. **Abdul Wahid Wahab** : Data curation, Investigation, Methodology, Software, Supervision, Validation. **Abdul Karim** : Writing – review & editing, Writing – original draft, Visualization, Validation, Supervision, Resources, Methodology, Conceptualization. **Fatimah** : Writing – review & editing, Writing – original draft, Visualization, Validation, Supervision, Resources, Methodology, Conceptualization.

Funding

The authors declare that no funds, grants, or other support were received during the preparation of this manuscript.

Data Availability

Data will be made available on request

Declaration of competing interest

The authors declare that they have no known competing financial interests or personal relationships that could have appeared to influence the work reported in this paper.

References

[1] AM Biasi, EA Takara, ML Scala-Benuzzi, AM Valverde and NN Gómez, Modification of electrodes with polymer nanocomposites: Application to the simultaneous determination of Zn(II), Cd(II), and Cu(II) in water samples, Analytica Chimica Acta. 1273, 341499 (2023). https://doi.org/10.1016/j.aca.2023.341499.

[2] Z. Lu, J. Zhang, W. Dai, X. Lin, J. Ye, J. Ye, A screen-printed carbon electrode modified with a bismuth film and gold nanoparticles for simultaneous stripping voltammetric determination of Zn (II), Pb (II) and Cu (II), Microchim. Acta. 184, 4731–4740 (2017). https://doi.org/10.1007/s00604-017-2521-8.

[3] P. Kamnoet, W. Aeungmaitrepirom, R.F. Menger, C.S. Henry, Highly selective simultaneous determination of Cu (II), Co (II), Ni (II), Hg (II), and Mn (II) in water samples using microfluidic paper-based analytical devices, Analyst. 146, 2229–2239 (2021). https://doi.org/10.1039/D0AN02200D.

[4] M. Hossain, D. Karmakar, S.N. Begum, S.Y. Ali, P.K. Patra, Recent trends in the analysis of trace elements in the field of environmental research: a review, Microchem. J. 165, 106086 (2021). https://doi.org/10.1016/j.microc.2021.106086.

[5] J. Wang, Stripping analysis at bismuth electrodes: a review, Electroanal. An Int. J. Devoted to Fundam. Pract. Asp. Electroanal. 17,1341–1346 (2005). https://doi.org/10.1002/elan.200403270.

[6] A Nourbakhsh, M. Rahimnejad, M. Asghary and H. Younesi, Simultaneous electro-determination of trace copper, lead, and cadmium in tap water by using silver nanoparticles and graphene nanoplates as a nanocomposite modified graphite electrode. Microchemical Journal. 176, 107137 (2022). https://doi.org/10.1016/j.microc.2021.107137.

[7] A. Abbas, H.M.A. Amin, Silver nanoparticles modified electrodes for electroanalysis: an updated review and a perspective, Microchem. J. 175, 10716 (2022). https://doi.org/10.1016/j.microc.2021.107166.

[8] K.B. Deore, S.B. Sitawar, N.N. Ingale, G.A. Bodke, M.L. Tsai, T. Hainik, M. D. Shirsat, Synergistic enhancement of electrochemical sensing: EDTA@AgNP's_ UIO-66 composite for sensitive and selective detection of toxic Hg(II) ions, Microchem. J. 209 (2025). https://doi.org/10.1016/j.microc.2025.112766.

[9] M. Satyanarayana, K.Y. Goud, K.K. Reddy, V.S. Kumar, K.V. Gobi, Silver nanoparticles impregnated chitosan layered carbon nanotube as sensor interface for electrochemical detection of clopidogrel in-vitro, Mater. Sci. Eng. C 101, 103–110 (2019). https://doi.org/10.1016/j.msec.2019.03.083.

[10] F. Hu, Y. Li, Y. Zhang, Y. Li, H. Li, S. Ai, Flexible Ag NCs/CNFs film for colorimetric and SERS dual-mode ultrasensitive detection of mercury ions (II), Vib. Spectrosc 118, 103342 (2022). https://doi.org/10.1016/j.vibspec.2022.103342.

[11] A.L. Suherman, K. Ngamchuea, E.E.L. Tanner, S.V. Sokolov, J. Holter, N.P. Young, R.G. Compton, Electrochemical detection of ultratrace (picomolar) levels of Hg using a silver nanoparticle-modified glassy carbon electrode, Anal. Chem. 89, 7166–7173 (2017). https://doi.org/10.1021/acs.analchem.7b01304.

[12] Lu, Silver nanomaterials sensing of mercury ions in aqueous medium, Coord. Chem. Rev. 456, 214363 (2022). https://doi.org/10.1016/j.ccr.2021.214363.
[13] I. Fatimah, H. Hidayat, B.H. Nugroho, S. Husein, Ultrasound-assisted biosynthesis of silver and gold nanoparticles using *Clitoria ternatea flower*, South African, J. Chem. Eng. 34, 97–106 (2020). https://doi.org/10.1016/j.sajce.2020.06.007.
[14] M. Sharma, D. Mourya, M. Choudhary, I. Goswami, M.P. Kundu, C.S.P. Dobhal, D. Tripathi, Guin, Thiol terminated chitosan capped silver nanoparticles for sensitive and selective detection of mercury (II) ions in water, Sensors Actuators, B Chem. 268, 310–318 (2018). https://doi.org/10.1016/j.snb.2018.04.121.
[15] O. Bozkaya, E. Arat, Z. Gun, Production and characterization of hybrid nanofiber wound dressing containing Centella asiatica coated silver nanoparticles by mutual electrospinning method, Eur. Polym. J. 166, 111023 (2022). https://doi.org/10.1016/j.eurpolymj.2022.111023.
[16] K. Maduray, R. Moodley, S. Ramdhani, R. Parboosing, The anti-HIV activity of biogenic silver nanoparticles synthesized from Centella asiatica extracts, J. Herb. Med. 35, 100592 (2022). https://doi.org/10.1016/j.hermed.2022.100592.
[17] E. Yanuar, K. Umam, W. Sarwana, I. Huda, D. Wijaya, R. Roto, M. Mudasir, Preparation and Vibrio sp antibacterial activity of silver nanoparticles mediated by chromolaena odorata leaf extract using different temperatures, Asian J. Biol. 14, 25–37 (2022). https://doi.org/10.9734/ajob/2022/v14i130203.
[18] P. Prema, V. Veeramanikandan, K. Rameshkumar, M.K. Gatasheh, A.A. Hatamleh, R. Balasubramani, P. Balaji, Statistical optimization of silver nanoparticle synthesis by green tea extract and its efficacy on colorimetric detection of mercury from industrial waste water, Environ. Res. 204, 111915 (2022). https://doi.org/ 10.1016/j.envres.2021.111915.
[19] S. Patra, A.K. Golder, R.V.S. Uppaluri, Ultrasensitive colorimetric detection and determination of Hg(II) using bioinspired AgNPs synthesized from mature Camellia sinensis leaves, Results Opt. 11 (2023). https://doi.org/10.1016/j. rio.2023.100411.
[20] A. Alam, A. Ravindran, P. Chandran, S. Sudheer Khan, Highly selective colorimetric detection and estimation of Hg2+ at nano-molar concentration by silver nanoparticles in the presence of glutathione, Spectrochim. Acta - Part A Mol. Biomol. Spectrosc. 137, 503–508 (2015). https://doi.org/10.1016/j. saa.2014.09.004.
[21] D.D. Yılmaz, D.A. Demirezen, H. Mıhçıokur, Colorimetric detection of mercury ion using chlorophyll functionalized green silver nanoparticles in aqueous medium, Surf. Interfaces 22, 1–7 (2021). https://doi.org/10.1016/j.surfin.2020.100840.
[22] A. Jabbar, A. Abbas, N. Assad, M. Naeem-Ul-Hassan, H.A. Alhazmi, A. Najmi, K. Zoghebi, M. Al Bratty, A. Hanbashi, H.M.A. Amin, A highly selective Hg2+ colorimetric sensor and antimicrobial agent based on green synthesized silver nanoparticles using Equisetum diffusum extract, RSC Adv. 13, 28666–28675 (2023). https://doi.org/10.1039/d3ra05070j.
[23] L. Mume, M. Kebede, D. Bekana, Z. Tan, M. Amde, Salvia tiliifolia leaf extract- based silver nanoparticles for colorimetric detection of Hg(II) in food and environmental samples, J. Food Compos. Anal. 133 (2024). https://doi.org/ 10.1016/j.jfca.2024.106426.
[24] C. Khelifi, R. Aitout, L. Makhloufi, S. Mahouche-Chergui, Eco-friendly synthesis of rGO/AgNPs hybrid nanomaterial for an efficient electrochemical sensor: simultaneous detection of paracetamol and caffeine in pharmaceuticals, Microchem. J. 212 (2025). https://doi.org/10.1016/j.microc.2025.113545.
[25] S. Ullah, R. Khalid, M.F. Rehman, M.I. Irfan, A. Abbas, A. Alhoshani, F. Anwar, H. M.A. Amin, Biosynthesis of phyto-functionalized silver nanoparticles using olive fruit extract and evaluation of their antibacterial and antioxidant properties, Front. Chem. 11, 1–14 (2023). https://doi.org/10.3389/fchem.2023.1202252.
[26] H. Sulistyarti, M.M. Utama, A.M. Fadhila, A. Cahyaningrum, R.J. Murti, A. Febriyanti, Green synthesis of silver nanoparticles using Coffea canephora fruit skin extract and its application for mercury detection in face cream samples, Anal. Sci. 39, 335–346 (2022). https://doi.org/10.1007/s44211-022-00237-w.
[27] G. Rajkumar, R. Sundar, Sonochemical-assisted eco-friendly synthesis of silver nanoparticles (AgNPs) using avocado seed extract: Naked-eye selective colorimetric recognition of Hg^{2+} ions in aqueous medium, J. Mol. Liq. 368 (2022). https://doi.org/10.1016/j.molliq.2022.120638.
[28] M Amare, A Worku, A Kassa and W Hilluf, Green synthesized silver nanoparticle modified carbon paste electrode for SWAS voltammetric simultaneous determination of Cd(II) and Pb(II) in Bahir Dar Textile discharged effluent. Heliyon. 6, e04401 (2020). https://doi.org/10.1016/j.heliyon.2020.e04401.
[29] C Pérez-Ràfols, JB Arrieta, N Serrano, JM Díaz-Cruz, C Ariño, J De Pablo and M Esteban, Ag nanoparticles drop-casting modification of screen-printed electrodes for the simultaneous voltammetric determination of Cu(II) and Pb(II). Sensors. 17, 1458 (2017). https://doi.org/10.3390/s17061458.
[30] M Zhou, L Han, D Deng, Z Zhang, H He, L Zhang and L Luo. 4-mercaptobenzoic acid modified silver nanoparticles-enhanced electrochemical sensor for highly sensitive detection of Cu^{2+}. Sensors and Actuators B: Chemical. 288, 45–54 (2019). https://doi.org/10.1016/j.snb.2019.04.060.

[31] Y Chen, H Li, C Fang, L Ai, J Chen, J Su, Q Zhang and Q Fu. Facile synthesis of reduced graphene oxide/silver nanoparticles composites and their application for detecting heavy metal ions, Journal of Alloys and Compounds .791, 117–124 (2019). https://doi.org/10.1016/j.jallcom.2019.01.320.
[32] I.O Wulandari, Pebriatin, B.E., Valiana, V., Hadisaputra, S., Ananto, A.D., Sabarudin, A. Green Synthesis of Silver Nanoparticles Coated by Water Soluble Chitosan and Its Potency as Non-Alcoholic Hand Sanitizer Formulation. Materials, 15, 4641 (2022). https:// doi.org/10.3390/ma15134641.
[33] S. Amin, M. Sher, A. Ali, M.F. Rehman, A. Hayat, M. Ikram, A. Abbas, H.M.A. Amin, Sulfonamide-functionalized silver nanoparticles as an analytical nanoprobe for selective Ni(II) sensing with synergistic antimicrobial activity, Environ. Nanotechnol. Monit. Manag. 18 (2022). https://doi.org/10.1016/j. enmm.2022.100735. https://doi.org/10.1016/j.enmm.2022.100735.
[34] A. Abbas, H.M.A. Amin, M. Akhtar, M.A. Hussain, C. Batchelor-McAuley, R. G. Compton, Supplementary Information Eco-friendly polymer succinate capping on silver nano-particles for enhanced stability: a UV-Vis and electrochemical particle impact study, Chem. Naissensis. 3, 71–91 (2020). https://doi.org/ 10.46793/chemn3.1.071a.
[35] A.L. Suherman, G. Zampardi, H.M.A. Amin, N.P. Young, R.G. Compton, Tannic acid capped gold nanoparticles: capping agent chemistry controls the redox activity, PCCP. 21, 4444–4451 (2019). https://doi.org/10.1039/C9CP00056A.
[36] D.V. Abere, S.A. Ojo, M.B. Paredes-Epinosa, A. Hakami, Derivation of composites of chitosan-nanoparticles from crustaceans source for nanomedicine: A mini review. Biomed. Eng. Adv. 4, 100058 (2022). https://doi.org/10.1016/j. bea.2022.100058.
[37] Wang, X. Zhou, S. Wu, S. Li, W. Wu, Z. Xiong, W. Shi, X. Tian, Q. Yu, Reusable surface plasmon resonance sensor for rapid detection of Cu2+ based on modified- chitosan thin film as an active layer, Sens. Actuators. 286, 59–67 (2019). https:// doi.org/10.1016/j.sna.2018.12.025.
[38] S. Zhang, S. Wei, H. Cheng, B. Rong, A highly sensitive colorimetric sensor for Hg2 + detection based on the oxidative enzyme mimics-like activity of hierarchical porous carbon@chitosan-modified silver nanoparticles, J. King Saud Univ. - Sci. 32, 1265–1271 (2020). https://doi.org/10.1016/j.jksus.2019.10.015.
[39] N.I.M. Fauzi, Y.W. Fen, N.A.S. Omar, S. Saleviter, W.M.E.M.M. Daniyal, H. S. Hashim, M. Nasrullah, Nanostructured chitosan/maghemite composites thin film for potential optical detection of mercury ion by surface plasmon resonance investigation. Polymers (basel). 12, 1–13 (2020). https://doi.org/10.3390/ polym12071497.
[40] J.H. Hwang, P. Pathak, X. Wang, K.L. Rodriguez, J. Park, H.J. Cho, W.H. Lee, A novel Fe-Chitosan-coated carbon electrode sensor for in situ As(III) detection in mining wastewater and soil leachate, Sensors Actuators, B Chem. 294, 89–97 (2019), https://doi.org/10.1016/j.snb.2019.05.044.
[41] R. Raghunandhan, L.H. Chen, H.Y. Long, L.L. Leam, P.L. So, X. Ning, C.C. Chan, Chitosan/PAA based fiber-optic interferometric sensor for heavy metal ions detection, Sensors Actuators, B Chem. 233, 31–38 (2016). https://doi.org/ 10.1016/j.snb.2016.04.020.
[42] J. Chen, Y. Chen, Y. Liang, Application of chitosan-N-doped graphene oxide ion- imprinted sensor in Cd (II) ions detection, Diam. Relat. Mater. 119, 108591 (2021). https://doi.org/10.1016/j.diamond.2021.108591.
[43] M.I. Hasan, Modification of Silver Nanoparticles with Polyvinyl Alcohol to Improve the Selectivity and Stability of Copper Metal (Cu) Indicators: A Trial on Red Macroalgae (*Happaphycus alvarezii*), *Thesis*, University of Indonesia, (2012).
[44] Y.K. Twu, Y.W. Chen, C.M. Shih, Preparation of Silver Nanoparticles Using Chitosan Suspensions, Powder Technology. 185, 251-257 (2008). https://doi.org/10.1016/j.powtec.2007.10.025.
[45] S.T Dubas, Panittamat K., Pranut P., Layer-by-layer deposition of antimicrobial silver nanoparticles on textile fibers, Colloids and Surfaces A : Physicochemical and Engineering Aspects, 289, 105-109 (2006). https://doi.org/10.1016/j.colsurfa.2006.04.012.
[46] S.J Wu, T.K Lin, W.C Chung, Huan C.Y., Heavy Metal Ion Colorimeter Sensors Using Ag Nanoparticles/Chitosan Aqueous Solution. *The 13th Asia Pasific Confederation of Chemical Engineering Congress*. 2010.
[47] K Liu, Q Wang and S Miah, Mercury (II) sensor based on nanosilver/chitosan modified screen-printed carbon electrode. Inorganic Chemistry Communications. 163, 113639 (2025). https://doi.org/10.1016/j.inoche.2024.113639.
[48] A. Maria C.G., Ananya S.A., Anitha V., Nidhin M, Ion-imprinted chitosan-stabilized biogenic silver nanoparticles for the electrochemical detection of arsenic (III) in water samples. New Journal of Chemistry, (2023). https://doi.org/10.1039/D2NJ04804C.
[49] RD Crapnell, CE Banks and DA Brownson, Electroanalytical Overview: screen-printed electrochemical sensing platforms. ChemElectroChem. 11, e202400370 (2024). https://doi.org/10.1039/d1sd00041a.
[50] P Taba, NY Parmitha and S Kasim. The synthesis of silver nanoparticles uses bay leaf extract (*Syzygium polyanthum*) as a bioreducer and tests its activity as an antioxidant. Indonesian Journal of Chemical Research. 7, 65–72 (2019).

[51] S Choudhary and S Yadav. 2020. Silver nanoparticle-modified electrodes for electrochemical sensing: Stability and performance considerations. Sensors and Actuators B: Chemical. 309, 1277 53 (2020). https://doi.org/10.1016/j.microc.2021.107166.
[52] I.O Wulandari, B.E. Pebriatin, V. Valiana, S. Hadisaputra, A.D. Ananto, A. Sabarudin, 2022. Green Synthesis of Silver Nanoparticles Coated by Water Soluble Chitosan and Its Potency as Non-Alcoholic HandSanitizer Formulation. *Materials*, 15, 4641 (2022). https:// doi.org/10.3390/ma15134641.
[53] R Munadi and Hutpriyanto. Identification of secondary metabolite compounds and antioxidant activity test of red ginger leaf extract (*Zingiber officinale rosc. Var. Rubrum*). Chemica : Scientific Journal of Chemistry and Chemistry Education. 24, 83-93 (2023). https://doi.org/10.35580/chemica.v24i2.56450.
[54] S Ceylan, E Yilmaz, M Yilmaz and M Soylak, Green synthesis of silver nanoparticles using plant extracts and their application in heavy metal sensing. Journal of Molecular Structure. 1234, 130118 (2021).
[55] E Gecer, G Akgül, D Yıldırım and N Yıldız. Electrochemical determination of heavy metals using modified carbon electrodes: A review. Electrochimica Acta. 403, 139689 (2022).
[56] JR Guimarães, FA Silva, MS Souza and AC Pereira, Silver nanoparticle-modified electrodes for electrochemical detection of Cd and Cu. Sensors and Actuators B: Chemical. 313, 128021 (2020).
[57] JM Hawar, MK Mohammed and HH Abdullah. Plant-mediated synthesis of silver nanoparticles and their analytical applications. Materials Today: Proceedings. 65, 120–126 (2022).
[58] H Jabbar, M Khan and S Rehman, Green-synthesized AgNPs for electrochemical sensing of heavy metals: A comprehensive review. Journal of Environmental Chemical Engineering. 8, 104519 (2020).
[59] SN Shah, R Ali, UA Khan and AZ Naqvi. Advances in silver nanoparticle-based electrochemical sensors for environmental monitoring. Analytical Methods. 12, 5400–5412 (2020).
[60] I Khan, K Saeed and I Khan. Nanoparticles: properties, applications and toxicities. Arabian Journal of Chemistry. 12, 908–931 (2019). 10.1016/j.arabjc.2017.05.011
[61] F Eker, E Akdaşçi, H Duman, M Bechelany and S Karav, Green synthesis of silver nanoparticles using plant extracts: a comprehensive review of physicochemical properties and multifunctional applications. International Journal of Molecular Sciences. 26, 6222 (2025). https://doi.org/10.3390/ijms26136222
[62] A Almuqrin, CJ Seneviratne, LJ Walsh and S Zafar, Tailored synthesis and profiling of capped silver and selenium nanoparticles for topical applications in paediatric dentistry. Dentistry Journal. 13, 456 (2025). https://doi.org/10.3390/dj13100456.
[63] MT Hamid, NN Hussein, GM Sulaiman and HA Mohammed, Antibacterial and antibiofilm properties of silver nanoparticles synthesized using Carthamus tinctorius extract against various multidrug-resistant bacterial strains. Discover Applied Science. 7, 548 (2025). https://doi.org/10.1007/s42452-025-06986-3.
[64] J Kesharwani, KY Yoon, J Hwang and M Rai. Phytofabrication of silver nanoparticles by leaf extract of Datura metel: hypothetical mechanism involved in synthesis. Journal of Bionanoscience, 39-44 (2009). https://doi.org/10.1166/jbns.2009.1008.
[65] S. Fiddaroini., Kurnia Indu, Moh. Farid R., Luailik M., Akhmad S., Chitosan-Coated silver nanoparticles with various floral honey bioreductors: A promising nonalcoholic hand gel sanitizer formulation. OpenNano. 21, 100228 (2025). https://doi.org/10.1016/j.onano.2024.100228
[66] S. Shinde, V. Folliero, A. Chianese, C. Zannella, A. DeFilippis, L. Rosati, M. Prisco, A. Falanga, A. Mali, M. Galdiero, Synthesis of Chitosan-Coated Silver Nanoparticle Bioconjugates and Their Antimicrobial Activity against Multidrug-Resistant Bacteria. Appl. Sci. 11, 9340 (2021). https:// doi.org/10.3390/app11199340.
[67] D.M. Cisterna, L. Chen, L. Bardehle, E. Hermosilla, G. Tortella, M. Chacón-Fuentes, O. Rubilar, Chitosan-Coated Silver Nanocomposites: Biosynthesis, MechanicalProperties, and Ag+ Release in Liquid and Biofilm Forms. Int. J. Mol. Sci. 26, 4130 (2025). https://doi.org/10.3390/ ijms26094130.
[68] M. Ghasemi, Mostafa G., Hajar R.L., Green synthesis of silver nanoparticles (AgNPs) and chitosan-coated silver nanoparticles (CS-AgNPs) using Ferula gummosa Boiss. gum extract: A green nano drug for potential applications in medicine. International Journal of Biological Macromolecules. (2025). https://doi.org/10.1016/j.ijbiomac.2024.138619
[69] M.M. Lopez, Lourdes G., Alberto J. L., Enrique N. Chitosan coated - biogenic silver nanoparticles from wheat residues as green antifungal and nanoprimig in wheat seeds. International Journal of Biological Macromolecules. 225, 964–973 (2023). https://doi.org/10.1016/j.ijbiomac.2022.11.159.
[70] S. Rajeshkumar, Munusamy T., Vijayarangan D.R., Naiyf S.A., Shine K., Jamal M.K., Kasi G., Natesan V., and Marimuthu G., Synthesis of greener silver nanoparticle-based chitosan nanocomposites and their potential antimicrobial activity against oral pathogens. Green Processing and Synthesis. 10, 658–665 (2021). https://doi.org/10.1515/gps-2021-0060.
[71] N. Willian, H. Pardi, S. Arief. Pembuatan dan Karakterisasi Nanopartikel Perak Menggunakan Ekstrak Buah Mangrove *Rhizophora stylosa*. Alchemy Jurnal Penelitian Kimia. 19, 56–60 (2023). https://doi.org/10.20961/alchemy.19.1.59359.53-60.
[72] S. Singla, A. Jana, R. Thakur, C. Kumari, S. Goyal, J. Pradhan, Green synthesis of silver nanoparticles using

Oxalis griffithii extract and assessing their antimicrobial activity. OpenNano. 7, 1–11 (2022). https://doi.org/10.1016/j.onano.2022.100047.

[73] F. Chen, Q. Zheng, X. Li, J. Xiong, Citrus sinensis leaf aqueous extract green-synthesized silver nanoparticles: Characterization and cytotoxicity, antioxidant, and anti-human lung carcinoma effects. Arabian Journal of Chemistry. 15, 1–10 (2022). https://doi.org/10.1016/j.arabjc.2022.103845.

[74] A.H. Khan, A.H., M. Zubair, Emerging technologies for the removal of heavy metals from wastewater, J. Hazard. Mater. 38, 121645 (2020). https://doi.org/10.1016/j. jece.2021.105688.

[75] S. Dangi, S., A. Gupta, D.K Gupta, S. Singh, N. Parajuli. Green synthesis of silver nanoparticles using aqueous root extract of *Berberis asiatica* and evaluation of their antibacterial activity. Chemical Data Collections. 28, 1–10 (2020). https://doi.org/10.1016/j.cdc.2020.100411.

[76] M.T. Yassin, F.O. Al-Otibi, A.A.F. Mostafa, A.A. Al-Askar, A. A. Facile Green Synthesis of Silver Nanoparticles Using Aqueous Leaf Extract of *Origanum majorana* with Potential Bioactivity against Multidrug Resistant Bacterial Strains. Crystals. 12, 1–18 (2022). https://doi.org/10.3390/cryst12050603.

[77] H. Yousaf, A. Mehmood, K.S Ahmad, M. Raffi. Green synthesis of silver nanoparticles and their applications as an alternative antibacterial and antioxidant agents. Materials Science and Engineering C. 112, 1–7 (2020). https://doi.org/10.1016/j.msec.2020.110901

[78] V. Kulikouskaya, H. Kseniya, Aliaksandr K., Irina K., Elena S., Ivan K., LijunYou, Vladimir A. Chitosan-capped silver nanoparticles : A comprehensive study of polymer molecular weight effect on the reaction kinetic, physicochemical properties, and synergetic antibacterial potential. Polymers. 3, 77–90 (2022). DOI:10.1002/pls2.10069.

[79] T.T.V Phan, D.T Phan, X.T Cao, T.C Huynh, J. Oh., Roles of Chitosan in Green Synthesis of Metal Nanoparticles for Biomedical Applications. Nanomaterials. 11, 273 (2021). https://doi.org/10.3390/ nano11020273.

[80] A.W. Wahab, A. Karim, N. La Nafie, P. Satrimafitrah, Triana, I.W. Sutapa. production of the nanoparticles using leaf of *Muntingia calabura L* . as bioreductor and potential as a blood sugar nanosensor. Journal of Physics: Conference Series.1242, 1–10 (2019). https://doi.org/10.1088/1742-6596/1242/1/012004

[81] R. Abbas, Luo, J., Qi, X., Naz, A., Khan, I.A., Liu, H., Yu, S., Wei, J., Silver Nanoparticles: Synthesis, Structure, Properties and Applications. Nanomaterials, 14, 1425 (2024). https://doi.org/10.3390/nano14171425.

[82] S. Kasim, P. Taba. The synthesis of silver nanoparticles uses the leaf extract of water hyacinth (*eichornia crassipes*) as a bioreducer. Covalent: Journal of Chemical Research. 6, 126–133 (2020).

[83] A.K. Roddu, A.W. Wahab, P. Taba, A. Ahmad. Silver Nanoparticle Produced by Using *Abelmoschus esculentus (L.)* Moench Leaves Extract Bioreduction Processs as Blood Glucose Nanosensor. Egyptian Journal of Chemistry, 65, 467–474 (2022). https://doi.org/10.21608/ejchem.2022.74382.3676

[84] S.S Al-Zahrania and Saleh Mohammed Al-Garnia., Antifungal potentiality of mycogenic silver nanoparticles capped with chitosan produced by endophytic Amesia atrobrunnea. Saudi Journal of Biological Sciences. 30, 103746 (2023). https://doi.org/10.1016/j.sjbs.2023.103746.

[85] E. Hermosilla. M. Diaz, J. Vera, M.J. Contreras, K. Leal, R. Salazar, L. Barrientos, G. Tortella, O. Rubilar., Antimicrobial synthesis of Chitosan-silver nanoparticles mediated by reusable Chitosan mushroom beads. Int. J. Mol. Sci. 24, 2318 (2023). https://doi.org/10.3390/ijms24032318.

[86] Y. Tkachenko and P Nieldzelski., FT-IR as a method for qualitative assessment of solid materials pitfalls from atmospheric CO_2 and H_2O. Molecules. 27, 8846 (2022). https://doi.org/10.3390/molecules27248846.

[87] X. Luo and C. Wang. Preparation and characterization of crosslinked chitosan nanoparticles. Journal of Applied Polymer Science. 127, 3590–3596 (2013).

[88] A.H. Jawad, S.S.A. Norrahma, B.H Hameed, K. Ismail. Chitosan-glyoxal film as a superior adsorbent for two structurally different reactive and acid dyes: adsorption and mechanism study. Int. J. Biol. Macromol. 135, 569–581 (2019). https://doi.org/10.1016/j.ijbiomac.2019.05.127.

[89] M Narayan, S Divya, D Natarajan, S Senthil-Nathan, S Kandasamy, A Chinnathambi, TA Alahmadi and A Pugazhendhi. Green synthesis of silver nanoparticles from aqueous extract of *Ctenolepis garcini L*. and assess their possible biological applications. Process Biochemistry, 107, 91-99 (2021). https://doi.org/10.1016/j.procbio.2021.05.008.

[90] H.K Akif, E. Olutas, F. Avcioglu, H. Kaya, B. Sahin. Quercetin- and caffeic acid-functionalized chitosan-capped colloidal silver nanoparticles: One-pot synthesis, characterization, and anticancer and antibacterial activities. Beilstein J. Nanotechnol. 14, 362–376 (2023). https://doi.org/10.3762/bjnano.14.31

[91] M. Costa, E. Carreiro, C. Filho, J. Sousa. 2025. Chitosan salts as stabilizing agents for the synthesis of silver nanoparticles (AgNPs). Chemistry Select. 8, e202203413 (2025). https://doi.org/10.1002/slct.202203413.

[92] M. Amare, A Worku, A Kassa and W Hilluf. Green synthesized silver nanoparticle modified carbon paste electrode for SWAS voltammetric simultaneous determination of Cd(II) and Pb(II) in Bahir Dar Textile discharged effluent. Heliyon, 6, e04401 (2020). https://doi.org/10.1016/j.sjbs.2023.103746

[93] A. Shehabeldine, S. Salem, O. Ali, K. Abd-Elsalam, F. Elkady, A. Hashem., Multifunctional Silver Nanoparticles Based on Chitosan: Antibacterial, Antibiofilm, Antifungal, Antioxidant, and Wound-Healing Activities. J. Fungi. 8, 612 (2022). https://doi.org/10.3390/jof8060612.

[94] P.K. Dara, R. Mahadevan, P.A Digita, S. Visnuvinayagam, L. Kumar, M. Suseela, C.N. Ravishankar, R. Anandan., Synthesis and biochemical characterization of silver nanoparticles grafted chitosan (Chi-Ag-NPs): In vitro studies on antioxidant and antibacterial applications. SN Appl. Sci. 2, 665 (2020). https://doi.org/10.1007/s42452-020-2261-y.

[95] A. Abdellatif, A. Abdelfattah, S. Aldalaan, H. Tawfeek. Chitosan-capped silver nanoparticles with potent and selective intrinsic activity against the breast cancer cells. Nanotechnol. Rev. 12, 20220546 (2023). https://doi.org/10.1515/ntrev-2022-0546.

[96] M. Naveed, B. Bukhari, T. Aziz, S. Zaib, M.A Mansoor, A.A. Khan, M. Shahzad, A.S Dablool, M.W. Alruways, A.A Almalki, A.S. Alamri, M. Alhomrani. Green Synthesis of Silver Nanoparticles Using the Plant Extract of *Acer oblongifolium* and Study of Its Antibacterial and Antiproliferative Activity via Mathematical Approaches. Molecules. 27, 1–15 (2022). https://doi.org/10.3390/molecules27134226.

[97] T. Malakhovska, A. Pogodin, M. Filep, A. Barannik, A. Kravets. Optical characteristics of silver-based nanocomposites fabricated by an environmentally friendly method. Semicond. Phys. Quantum. Electron. 26, 076–083 (2023). https://doi.org/10.15407/spqeo26.01.076.

[98] S.O. Aisida, K. Ugwu, P.A Akpa, A.C. Nwanya, U. Nwankwo, S.S. Botha, P.M. Ejikeme, I. Ahmad, M. Maaza, F.I. Ezema., Biosynthesis of silver nanoparticles using bitter leave (*Veronica amygdalina*) for antibacterial activities. Surfaces and Interfaces, (2019). https://doi.org/10.1016/j.surfin.2019.100359.

[99] E. Mirda, R. Idroes, K. Khairan, T.E. Tallei, M. Ramli, N. Earlia, A. Maulana, G.M Idroes, M. Muslem, Z. Jalil., Synthesis of Chitosan-Silver Nanoparticle Composite Spheres and Their Antimicrobial Activities. *Polymers*, 13, 3990 (2021). https:// doi.org/10.3390/polym13223990.

[100] L.S Wang, C.Y. Wang, C.H. Yang, C.L. Hsieh, S.Y. Chen, J.J Wang, K.S. Huang. Synthesis and anti-fungal effect of silver nanoparticles–chitosan composite particles. Int. J. Nanomed. 10, 2685 – 2696 (2015). https://doi.org/10.2147/IJN.S77410.

[101] MR Bindhu, M Umadevi, GA Esmail, NA Al-Dhabi and MV Arasu. Green synthesis and characterization of silver nanoparticles from *Moringa oleifera* flower and assessment of antimicrobial and sensing properties. Journal of Photochemistry and Photobiology B: Biology, 205, 111836 (2020). https://doi.org/10.1016/j.jphotobiol.2020.111836.

[102] V.S Suvith and D. Philip. Catalytic Degradation Of Methylene Blue Using Biosynthesized Gold and Silver Nanoparticles, Spectrochim Acta A Mol Biomol Spectrosc. 118, 526-532 (2014). https://doi.org/10.1016/j.saa.2013.09.016.

[103] K. Jeeva, M. Thiyagarajan, V. Elangovan, N. Geetha, P. Venkatachalam. *Caesalpinia coriaria* Leaf Extract Mediated Biosynthesis of Metallic Silver Nanoparticles and Their Antibacterial Activity Against Clinically Isolated Pathogens. Ind Crops Prod. 52, 714-720 (2014). https://doi.org/10.1016/j.indcrop.2013.11.037.

[104] C. Vishwasrao, B. Momin, and L. Ananthanarayan. Green Synthesis Of Silver Nanoparticles Using Sapota Fruit Waste And Evaluation Of Their Antimicrobial Activity, Waste and Biomass Valorization. 10, 2353-2363 (2019). https://doi.org/10.1007/s12649-018-0230-0.

[105] S. Palithya, S.A. Gaddam, V.S. Kotakadi, J. Penchalaneni, V.N. Challagundla. Biosynthesis of silver nanoparticles using leaf extract of decaschistia crotonifolia and its antibacterial, antioxidant, and catalytic applications. Green Chem. Lett. Rev. 14, 136–151 (2021). https://doi.org/10.1080/17518253.2021.1876172

[106] T. Tang, T. Hai-Anh Nguyen, C. Minh Tran, V. Khanh Doan, N. Nguyen, B. Thanh Vu, N. Dang, T. Tu Duong, V. Hung Pham, L. Dai Tran, T. Van Vo, T. Nguyen, Fabrication of silver nanoparticle-containing electrospun polycaprolactone membrane coated with chitosan oligosaccharides for skin wound care, Journal of Science: Advanced Materials and Devices, 8, 100582 (2023). https://doi.org/10.1016/j.jsamd.2023.100582.

[107] L.C Lu, C.I Wang, W.F Sye. Applications of chitosan beads and porous crab shell powder for the removal of 17 organochlorine pesticides (OCPs) in water solution. Carbohydr. Polym. 83, 1984–1989 (2011). https://doi.org/10.1016/j.carbpol.2010.11.003.

[108] R,C Mishra, R. Kalra, R. Dilawari, M. Goel, C.J Barrow. Biosynthesis of *Aspergillus terreus* Mediated Gold Nanoparticle: Antimicrobial, Antioxidant, Antifungal and In Vitro Cytotoxicity Studies Rahul. Materials, 15, 1–19 (2022). https://doi.org/10.3390/ma15113877.

[109] M.M Ilmi. Nadya N., Evi M., Pindi S., Ismunandara., Journal of Research and Development on Nanotechnology X-ray Diffraction Peak Profile Analysis for Determination of Microstructural Properties of Hematite (Fe_2O_3), (2021). 10.5614/jrdn.2021.1.1.16667.

[110] N.M. Escobar, Daniel O.A, Jorge A. V, Catalina G., Angélica S.G, Piedad F., Gañan R, Lina M.V. A, Juan P.E, Natalia C., Omar T., Robin Z.G, Pablo M S. Use of Fourier Series in X-ray Diffraction (XRD)

Analysis and Fourier-Transform Infrared Spectroscopy (FTIR) for Estimation of Crystallinity in Cellulose from Different Sources. Polymers (Basel), 14, 5199 (2022). doi: 10.3390/polym14235199.

[111] Ali, H., Azad, A. K., Khan, K. A., Rahman, O., Chakma, U., & Kumer, A., Analysis of Crystallographic Structures and Properties of Silver Nanoparticles Synthesized Using PKL Extract and Nanoscale Characterization Techniques. ACS Omega, 8, 28133–28142 (2023). https://doi.org/10.1021/acsomega.3c01261.

[112] U. Holzwarth, Gibson, N. The Scherrer equation versus the 'Debye-Scherrer equation'. Nature Nanotech, 534, 6 (2011). https://doi.org/10.1038/nnano.2011.145

[113] M. Sirajuddin, M. Synthesis of Silver Nanoparticles Using Nutmeg Seed Essential Oil (*Myristica fragrans houtt*) and Its Application as a Lichen Growth Inhibitor on Rocks. Thesis, Islamic University of Indonesia, Yogyakarta, (2022).

[114] J.A Seyforth. Scanning electron microscopy (SEM): an introduction to the use of SEM for characterising the surface topology and composition of matter with further applications. Exp. Tech. Condens. Matter Phys. (2015). https://www.researchgate.net/publication/30424740.

[115] Yoshizuka K, Lou Z, Inoue K. Silver-complexed chitosan microparticles for pesticide removal. React Funct Polym. 44, 47–54 (2000). https://doi.org/10.1016/S1381-5148(99)00076-0.

[116] Govindan S, Nivethaa EAK, Saravanan R, Narayanan V, Stephen A. Synthesis and characterization of chitosan–silver nanocomposite. Appl Nanosci. 2, 299–303 (2012). 10.1007/s13204-012-0109-5.

[117] M. Oves, M. Ahmar Rauf, M. Aslam, H.A Qari, H. Sonbol, I. Ahmad, G. Sarwar Zaman, M. Saeed. Green synthesis of silver nanoparticles by *Conocarpus Lancifolius* plant extract and their antimicrobial and anticancer activities. Saudi Journal of Biological Sciences, 29, 460–471 (2022). https://doi.org/10.1016/j.sjbs.2021.09.007.

[118] C. Singh, J. Kumar, P. Kumar, B.S. Chauhan, K.N Tiwari, S.K Mishra, S. Srikrishna, R. Saini, G. Nath, J. Singh. Green synthesis of silver nanoparticles using aqueous leaf extract of *Premna integrifolia (L.)* rich in polyphenols and evaluation of their antioxidant, antibacterial and cytotoxic activity. Biotechnology and Biotechnological Equipment, 33, 359–371 (2019). https://doi.org/10.1080/13102818.2019.1577699.

[119] F. Laghrib. N. Ajermouna, M. Bakasseb, S.Lahricha, M.A. El Mhammedia. Synthesis of silver nanoparticles assisted by chitosan and its application to catalyze the reduction of 4-nitroaniline. International Journal of Biological Macromolecules. 135, 752–759 (2019). https://doi.org/10.1016/j.ijbiomac.2019.05.209.

[120] A.Franconetti, J.M. Carnerero, R. Prado-Gotor, F. Cabrera-Escribano, C. Jaime. Chitosan as a capping agent: insights on the stabilization of gold nanoparticles, Carbohydr. Polym. 207, 806–814 (2019). https://doi.org/ 10.1016/j.carbpol.2018.12.046.

[121] W. Wang, P. Ma, Q. Zhao, M. Liu, Y. Zheng., Beneficial properties of the biosynthesized silver/chitosan nanoparticles mediated by Mentha piperita in rats with heart failure following myocardial infarction. *Inorg. Chem. Commun.* 141, 109581 (2022). https://doi.org/10.1016/j.inoche.2022.109581.

[122] K. Jemal, B.V Sandeep, S. Pola. Synthesis, Characterization and Evaluation of The Antibacterial Activity of *Allophylus serratus* Leaf and Leaf Derived *Callus Extracts* Mediated Silver Nanoparticles, J. Nanometer. 1-12 (2017), https://doi.org/10.1155/2017/4213275

[123] P. Pasakon, V. Primpray, J. Thangphatthanarungruang, W. Kamsong, A. Wisitsoraat, W. Laiwattanapaisal, V. Intasanta, C. Karuwan., Conductive disposable screen-printed graphene oxide-molybdenum disulfide electrode for electrochemical sensing applications, Electrochem. Commun. 166 (2024). https:// doi.org/10.1016/j.elecom.2024.107778.

[124] S.N. Jolge, A.A. Ensafi, B. Rezaei., Ultra-sensitive electrochemical aptasensor based on zeolitic imidazolate framework-8 derived Ag/Au core-shell nanoparticles for mercury detection in water samples, Sensors Actuators, B Chem. 331, 129426 (2021). https://doi.org/10.1016/j.snb.2020.129426

[125] Liu, K., Qihui W., Sakil M., Mercury (II) sensor based on nanosilver/chitosan modified screen-printed carbon electrode, Inorganic Chemistry Communications. (2025). https://doi.org/10.1016/j.inoche.113639

[126] Imran, M., Christopher J. E., Massimo F. Bertino, Muhammad R. Shah and Vamsi K. Yadavalli., Chitosan Stabilized Silver Nanoparticles for the Electrochemical Detection of Lipopolysaccharide: AFacile Biosensing Approach for Gram-Negative Bacteria. Micromachines. 11, 413 (2020). 10.3390/mi11040413.

[127] Chen, J., Y. Chen, Y. Liang., Application of chitosan-N-doped graphene oxide ion- imprinted sensor in Cd (II) ions detection, Diam. Relat. Mater. 119, 108591 (2021). https://doi.org/10.1016/j.diamond.2021.108591.

[128] O.S Ivanova, Francis P. Zamborini. Size-Dependent Electrochemical Oxidation of Silver Nanoparticles. Journal of the American Chemical Society 131, 958–964 (2009). https://doi.org/10.1021/ja908780g

[129] C.A Little, Christopher B., Kamonwad N., Chuhong Lin, Neil P Young [1], Richard G Compton. 2018. Coupled Optical and Electrochemical Probing of Silver Nanoparticle Dissolution. Chemistry Open, 7, 370–380 (2018). 10.1002/open.201800048.

[130] H. Luo, Xu Ji, Shuang Cheng. Investigation into the electrochemical behaviour of silver in alkaline versus neutral media. RSC Advances 10, 8453–8459 (2020). 10.1039/c9ra10282e.

[131] J. Dolińska, Marcin H., Robert A., Anna M., Grzegorz M., Marcin P., Marcin O., Effect of the medium on electrodissolution of adsorbed silver nanoparticles. Electrochimica Acta. (2020) https://doi.org/10.1016/j.electacta.2020.136406.

[132] Yulirohyami, Gani P., Is Fatimah, Dwi Siswantaa, Mudasir M., Green synthesis of AgNPs-dithizone@chitosan for highly selective and reusable electrochemical sensors of Hg^{2+}. Microchemical Journal. 214, 114015 (2025). https://doi.org/10.1016/j.microc.2025.114015.

[133] G. Vyas, S. Bhatt, P. Paul. Synthesis of calixarene-capped silver nanoparticles for colorimetric and amperometric detection of mercury Hg (II) , Hg (0), ACS Omega. 3860–3870 (2019). https://doi.org/10.1021/acsomega.8b03299

[134] Shehzad, T.J., M. Shezad, M. Aamir, H. Hussain. Threonine based electrochemical sensor for micro level sensing of mercuric ions in aqueous bodies, Meas. J. Int. Meas. Confed. 183, 109775 (2021). https://doi.org/10.1016/j. measurement.2021.109775**.**

[135] H. Darmokoesoemo, Khasanah. M., Kustyarini, L., Kadmi, Y., Elmsellem, H. and Kusuma, H. S.,. Development of electrode carbon paste/molecularly imprinted polymer (MIP) with methacrylic acid as monomer to analyze glucose by potentiometry. Results in Physics, 7, 1781–1791 (2017). 10.1016/j.rinp.2017.05.015.

[136] R Tahaei, H Shayani-Jam and MR Yaftian. Voltammetric determination of trace copper (II), cadmium (II), and lead (II) using a Schiff base modified glassy carbon working electrode. Monatshefte für Chemie.152 , 51–59 (2021).

[137] DC Harris. Quantitative chemical analysis. 9th ed. (W. H. Freeman and Company, New York, 2015).

[138] J Wang. Analytical Electrochemistry. 3rd ed. (Wiley, New Jersey, 2006).

[139] AJ Bard and LR Faulkner. Electrochemical Methods: Fundamentals and Applications. 2nd ed. (Wiley, New Jersey, 2001).

[140] A Shrivastava and VB Gupta. Methods for the determination of limit of detection and limit of quantitation. Chronicles of Young Scientists. 2, 21–25 (2011). https://doi.org/10.4103/2229-5186.79345.

[141] Y Li, H Zhang and J Wang. Nanostructured electrode materials for electrochemical detection of heavy metals. Electrochimica Acta. 296, 1100–1112 (2019).

[142] A Dzhan. Stability and surface behavior of silver nanoparticles under ambient storage conditions. Journal of Nanomaterials Research. 14, 215–224 (2012).

[143] DS Ben Ali, F Krid, AS Saadi, M Nacef and ML Chelaghmia. Simultaneous electrochemical detection of Cd^{2+} and Pb^{2+} using a green silver nanoparticle/polyaniline-modified carbon paste electrode. RSC Advances.15, 29654-29665 (2025). https://doi.org/10.1039/d5ra03135d.

[144] P Blaubaum. Silver nanoparticle–modified electrodes for heavy-metal electrochemical sensing: A review. Journal of Electrochemical Analysis. 45, 215–229 (2020).

[145] A Jiménez, MBG García, DH Santos and PF Bolado. Screen-Printed Electrodes Modified with Metal Nanoparticles for Small Molecule Sensing. Biosensors. 10, 9 (2020). https://doi.org/10.3390/bios10020009.

[146] M Rubino, L Rossi and A Bianchi. Enhancement of metal-ion preconcentration and sensitivity in screen-printed electrodes using ultrasmall metal nanoparticles. Journal of Electroanalytical Science. 128, 345–356 (2023). https://doi.org/10.1016/j.talo.2023.100203.

[147] N Mphuthi, LM Sikwhivhilu, SS Ray and B Ntsendwana., Electrooxidation of dopamine using MoS_2-Ag conductive ink on screen-printed electrodes for electrochemical sensing. Frontiers in Sensors. 6, 1650004 (2025). https://doi.org/10.3389/fsens.2025.1650004.

[148] AE Kartika, H Setiyanto, RV Manurung, SNA Jenie and V Saraswaty. Silver nanoparticles coupled with graphene nanoplatelets modified screen-printed carbon electrodes for rhodamine b detection in food products. ACS Omega. 6, 31477-31484 (2021). https://doi.org/10.1021/acsomega.1c03414.

[149] MB Gholivand and A Pourhossein. Simultaneous determination of copper and cadmium in environmental water and tea samples by adsorptive stripping voltammetry. Talanta. 93, 129–135 (2012). https://doi.org/10.3906/kim-1004-553.